Marine Geology 385 (2017) 304–327

Contents lists available at ScienceDirect

Marine Geology

journal homepage: www.elsevier.com/locate/margo

Invited review article

Benthic storms, nepheloid layers, and linkage with upper ocean dynamics in the western North Atlantic

Wilford D. Gardner [a,*], Brian E. Tucholke [b], Mary Jo Richardson [a], Pierre E. Biscaye [c]

[a] Texas A&M University, College Station, TX 77845, USA
[b] Woods Hole Oceanographic Institution, Woods Hole, MA 02543, USA
[c] Lamont-Doherty Earth Observatory of Columbia University, Palisades, NY 10964, USA

ARTICLE INFO

Article history:
Received 20 July 2016
Received in revised form 20 December 2016
Accepted 30 December 2016
Available online 10 January 2017

Keywords:
Benthic storms
Benthic nepheloid layer
Abyssal currents
Seafloor erosion
Eddy kinetic energy
Cyclogenesis

ABSTRACT

Benthic storms are episodic periods of strong abyssal currents and intense, benthic nepheloid (turbid) layer development. In order to interpret the driving forces that create and sustain these storms, we synthesize measurements of deep ocean currents, nephelometer-based particulate matter (PM) concentrations, and seafloor time-series photographs collected during several science programs that spanned two decades in the western North Atlantic. Benthic storms occurred in areas with high sea-surface eddy kinetic energy, and they most frequently occurred beneath the meandering Gulf Stream or its associated rings, which generate deep cyclones, anticyclones, and/or topographic waves; these create currents with sufficient bed-shear stress to erode and resuspend sediment, thus initiating or enhancing benthic storms. Occasionally, strong currents do not correspond with large increases in PM concentrations, suggesting that easily erodible sediment was previously swept away. Periods of moderate to low currents associated with high PM concentrations are also observed; these are interpreted as advection of PM delivered as storm tails from distal storm events. Outside of areas with high surface and deep eddy kinetic energy, benthic nepheloid layers are weak to non-existent, indicating that benthic storms are necessary to create and maintain strong nepheloid layers. Origins and intensities of benthic storms are best identified using a combination of time-series measurements of bottom currents, PM concentration, and bottom photographs, and these should be coupled with water-column and surface-circulation data to better interpret the specific relations between shallow and deep circulation patterns. Understanding the generation of benthic nepheloid layers is necessary in order to properly interpret PM distribution and its influence on global biogeochemistry.

Contents

* Corresponding author.
E-mail addresses: wgardner@ocean.tamu.edu (W.D. Gardner), btucholke@whoi.edu (B.E. Tucholke), mrichardson@ocean.tamu.edu (M.J. Richardson), biscaye@ldeo.columbia.edu (P.E. Biscaye).

http://dx.doi.org/10.1016/j.margeo.2016.12.012

1. Introduction

Jerlov (1953) reported the discovery of cloudy (turbid) layers near the seafloor using optical measurements, and he summarized views that these layers might be generated by earthquakes (later shown to generate submarine slides and turbidity currents), volcanic eruptions, or seafloor erosion by strong bottom currents. Ewing and Thorndike (1965) called these turbid bottom waters "nepheloid layers" (from the Greek word "nephos", meaning cloud) and stated that "the nepheloid layer is a permanent and widespread feature, not a transitory response to a storm or earthquake nor restricted to the vicinity of a submarine canyon."

The spatial variability of the benthic nepheloid layer (hereafter 'nepheloid layer') in the Atlantic Ocean was mapped by Eittreim et al. (1976) based on an optical index using Lamont-Doherty nephelometer data (Thorndike, 1975). Biscaye and Eittreim (1977) converted this optical index to particulate matter (PM) concentrations using the measured mass of particles filtered from water samples collected from hydrographic casts at the depths where the optical measurements were made. From samples taken over a 12-year period they found that near-bottom PM concentrations varied spatially by a factor of 70 across the western North Atlantic Basin, with the highest concentrations near the western margin of the basin (Fig. 1). They suggested that the strong nepheloid layer at the margin was caused by seafloor erosion beneath the Deep Western Boundary Current (DWBC), the cold, deep southward flow of bottom water formed at high latitudes in the North Atlantic. Tucholke and Eittreim (1974) examined the nepheloid layer in the southern part of the basin over the Greater Antilles Outer Ridge and the Puerto Rico Trench. The layer there is in Antarctic Bottom Water (AABW) that underlies and generally follows the path of the DWBC, and it is much weaker than the nepheloid layer to the northwest.

Heezen and Hollister (1972, pp. 358–359) suggested that, in addition to mean currents near the sea floor, perturbations from deep eddy-type flows could affect seafloor erosion, suspension, and advection of sediment. Laine (1977) and Laine and Hollister (1981) noted that the strongest nepheloid layers corresponded closely with the mean circulation of a deep gyre system in the basin as proposed by Worthington (1976) and further explained by Hogg (1983) and Hogg et al. (1986). These ideas about patterns of deep circulation have been supported by subsequent models and current measurements (Arbic et al., 2009, 2010; Wright et al., 2013) and are reviewed in detail by Turnewitsch et al. (2013).

Much of what has been inferred about patterns of bottom currents and their effects in eroding and transporting sediment is taken from extensive compilations of bottom photographs that exhibit bedforms and show relative intensity and direction of currents (e.g., Heezen and Hollister, 1972; Hollister and Heezen, 1972; Tucholke et al., 1973, 1985; Hollister and McCave, 1984; McCave and Tucholke, 1986; Hollister and Nowell, 1991). Unfortunately, individual photographs provide little or no information about timing of current events and they have rarely been coupled with direct measurements of currents or bottom-water turbidity.

It wasn't until the late 1970's and early 1980's that time-series measurements of bottom currents were made simultaneously with moored nephelometers for periods longer than a week (Johnson et al., 1976). Large, episodic increases in bottom-water turbidity in the deep ocean were first documented in long time-series measurements (2.5-month duration) using a long-term nephelometer (LTN) moored 20 m above the seafloor on the northwestern Bermuda Rise in the Western North Atlantic (Gardner and Sullivan, 1981). They coined the term "benthic storms" to describe these events. Similar events were later intensely studied on the lower continental rise south of Nova Scotia during the High Energy Benthic Boundary Layer Experiment (HEBBLE) (Hollister and McCave, 1984; Gardner et al., 1985a; Hollister and Nowell, 1991; Pak, 1983; Pak and Zaneveld, 1983; Grant et al., 1985); they have also been studied on the lowermost continental rise and Hatteras Abyssal Plain off the eastern United States (Isley et al., 1990), in the northeast Atlantic (Klein and Mittelstaedt, 1992), and in the Argentine Basin (Richardson et al., 1993). Benthic storms are analogous to dust storms in that the fluid (air/water) moves fast enough to erode and resuspend the underlying sediment, mixing it with the overlying fluid to create clouds of dust/PM that are redistributed downwind/downstream.

McCave (1986) summarized the state of research on nepheloid layers 30 years ago, and since then numerous studies have contributed to understanding their origin and development. Nonetheless, major questions remain: How ubiquitous, variable or persistent are nepheloid layers? What primary driving forces create and maintain the layers? How do surface-water circulation (e.g., the Gulf Stream) and deep-water currents (e.g., the DWBC) affect nepheloid layers? How frequent and intense are benthic storms? Are sustained high current speeds required to both initiate and maintain nepheloid layers or are they generated and maintained primarily by intermittent benthic storms?

In this paper, we first review known characteristics and proposed origins of the permanent nepheloid layer, and we then investigate how

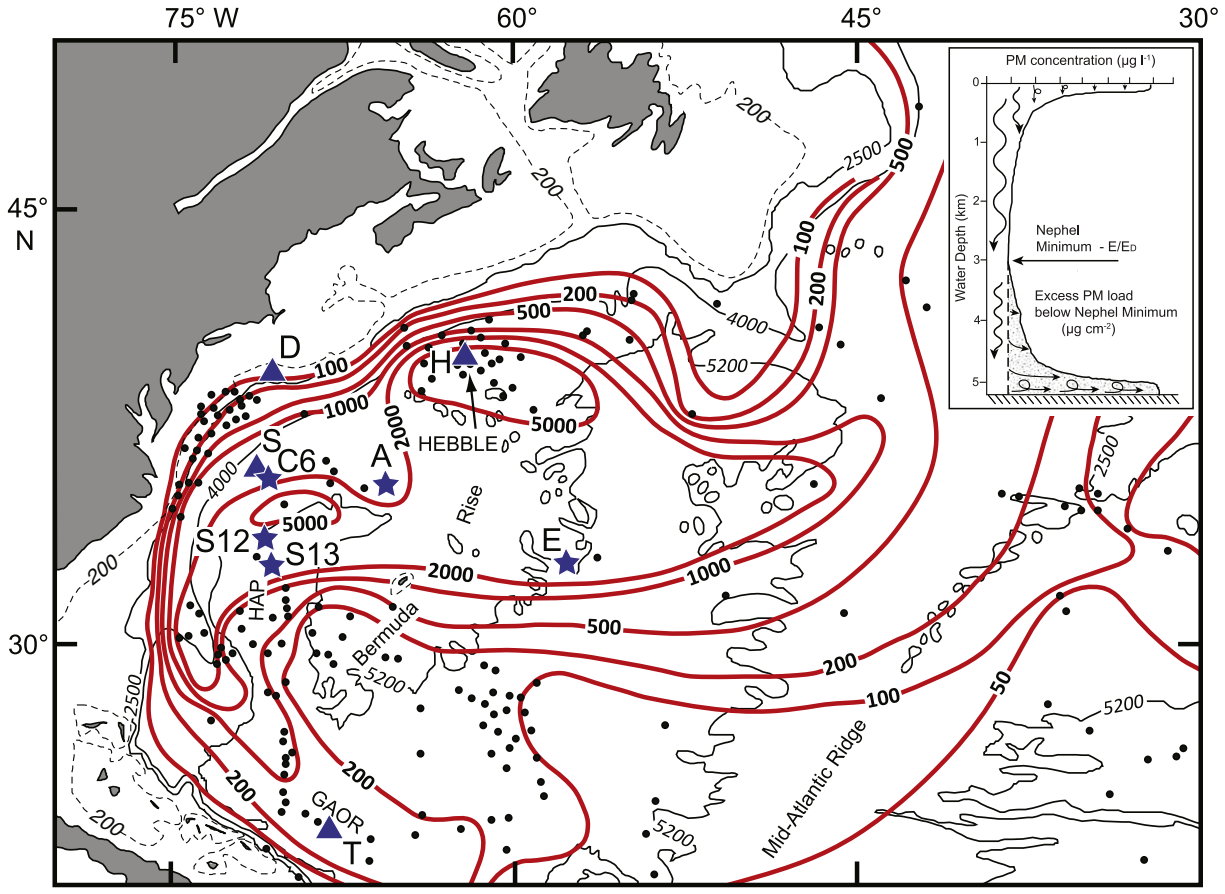

Fig. 1. Distribution of excess particulate matter load (red contours, in μg cm^{-2}) in the benthic nepheloid layer in the western North Atlantic Ocean, updated from Biscaye and Eittreim (1977) with nephelometer data from the HEBBLE area. Nephelometer profile locations are indicated by dots. BOM locations (triangles) and mooring sites (stars) are identified (C6 is current-meter mooring CMME-6). Black dashed and solid lines are bathymetric contours (200, 2500, 4000, and 5200 m). GAOR: Greater Antilles Outer Ridge, HAP: Hatteras Abyssal Plain, HEBBLE: location of the High Energy Benthic Boundary Layer Experiment. The insert shows an idealized nephelometer profile, depth of the nephel minimum, and a dotted area that is excess PM load below that minimum. Looping arrows indicate surface-water and benthic boundary layer mixing. Horizontal arrows indicate lateral transport of resuspended sediment from surrounding topography. Wavy vertical arrows indicate particles sinking from surface waters.

benthic storms (as observed in combined time-series measurements of currents, light scattering from a long-term nephelometer, and bottom photographs) relate to this layer. The time-series measurements were obtained in months- to year-long deployments of a Bottom Ocean Monitor (BOM) and other moorings. We compare these records with 1) the distribution and intensity of nepheloid layers in the western North Atlantic, 2) observed patterns of surface and abyssal eddy kinetic energy (EKE), and 3) the location of Gulf Stream rings and meanders during benthic storms. Our results provide important new insights into the creation, persistence, and decay of nepheloid layers. Because PM in these layers scavenges trace elements and their isotopes from the water column, our results also provide key information that will be useful to GEOTRACES (Anderson et al., 2014; Hayes et al., 2014) and other programs that investigate physical and bio-geochemical processes where PM concentrations are critical for understanding water column and sediment-water interactions.

2. Background

2.1. PM load in the benthic nepheloid layer

A first-order question is what quantity of PM is actually contained in the nepheloid layer, and what thickness of sediment would result if all PM in the layer settled out? As mapped by Biscaye and Eittreim (1977), the gross PM load in a nepheloid layer (μg cm^{-2}) includes both PM settling from surface waters and PM resuspended locally or advected into the area. The excess (resuspended/advected) load, termed the net particulate standing crop by Biscaye and Eittreim (1977), is the total PM load in the nepheloid layer minus the PM from surface waters as approximated by the value of the nephel minimum (Fig. 1 inset). Assuming a density of 1.4 g cm^{-3} for unconsolidated surface sediments (Tucholke and Shirley, 1979), the thickness of a layer of sediment that could be deposited from the excess load, based on contours in Fig. 1 (50–5000 μg cm^{-2}), would range from 0.36 μm for the relatively clear bottom water in the central North Atlantic to 36 μm along the western portion of the basin. The nepheloid layer at a few stations in the HEBBLE area, which yielded the highest particle concentration ever measured in the deep ocean (12,700 μg l^{-1}), could deposit up to 120 μm of sediment. Thus, erosion of only very thin layers of sediment is sufficient to produce most nepheloid layers in the ocean basins. However, to sustain the nepheloid layer, PM must either be continually mixed in the bottom water or episodically replenished by seafloor erosion.

2.2. PM grain size and composition in the nepheloid layer and relation to seafloor sediments

Filtered water samples collected <200 m above bottom (mab) in the North Atlantic during the GEOSECS program showed that 40–80% of particles were clay-size (<2 μm) (Bishop and Biscaye, 1982). These authors also found that the composition of the particles matched the composition of the underlying sediment.

In the HEBBLE study area, Coulter Counter measurements of particle-size distribution in water from the nepheloid layer showed peaks at 4–8 μm and sometimes a secondary peak between 20 and 60 μm that was likely composed of aggregates (McCave, 1985; Richardson and Gardner, 1985). Gentle wet-sieving of particles collected in sediment traps < 500 mab in the HEBBLE area and on the adjacent Sohm Abyssal Plain showed that 40–80% were <20 μm and 15–40% were 20–63 μm (Gardner et al., 1983; Gardner and Richardson, 1992); however, it is likely that much of the material entered the traps as larger aggregates that later broke up in the trap and/or during processing. The percentage of organic carbon in traps < 200 mab was 0.4–1.2% of the sample compared with 2.2–4.1% for traps 500–1500 mab at the same site; this most likely was because material in near-bottom traps contained a higher percentage of resuspended material than material settling from surface waters (Gardner et al., 1983, 1985b).

At two sites on the middle and upper continental rise south of the Hudson Canyon off New Jersey, elemental composition of particles sampled from the nepheloid layer in traps within 30 mab closely agreed with composition of seafloor sediments for most elements (Gardner et al., 1985b). Gentle wet sieving of one core-top yielded 35% <20 μm, 35% 20–63 μm, and 30% >63 μm. Farther south over the Greater Antilles Outer Ridge, PM filtered from water samples from the nepheloid layer was 15% <2 μm, with a mean grain size of ~3–4 μm (Tucholke, 1975). PM in the nepheloid layer there had a composition similar to underlying seafloor sediments, and chlorite content of both the PM and the sediment suggested long-term, long-distance transport from a source along the northeastern margin of North America.

Overall, filtered water and sediment-trap samples show that most particles in the nepheloid layer are in the fine-silt to clay-size range (less than about 8 μm) and include very little organic carbon. Similar composition of PM and underlying seafloor sediment also suggests episodic deposition and resuspension of material from the local seabed.

2.3. PM from submarine canyons and continental shelves

Although Ewing and Thorndike (1965) recognized that turbidity currents exiting submarine canyons could not account for the permanent nepheloid layer, there is at least one documented instance where a turbidity current may have contributed to the layer. Amos and Gerard (1979) measured very high PM and elevated O_2, temperature (T), and salinity (S) in the bottom mixed layer (BML) at one station south of the Grand Banks, and they suggested that they sampled the tail end of a turbidity current there.

More recently, it has been found that winter cooling and convective mixing in the western Mediterranean (Canals et al., 2006; Palanques et al., 2009; Puig et al., 2013b) can increase water density enough to cause cascading down canyons, the continental slope, or even in the open Mediterranean (Houpert et al., 2016). Water cascading down the margins entrains sediment and transports it to depths > 2400 m, thus creating nepheloid layers as thick as 1500 m. Winter storms can enhance this process. Similar cooling and cascading phenomena have been measured at high latitudes off eastern Canada (Puig et al., 2013a). A different mechanism for supplying PM to deep water has been observed in the subtropics off southern Taiwan, where torrential rainfall created sufficiently high PM concentrations in the Gaoping River to generate turbid hyperpycnal flows down Gaoping Canyon to depths > 3500 m (Kao et al., 2010).

In addition to acting as conduits for turbidity currents and other density flows, submarine canyons play a role in moving sediment beyond the continental slope and rise due to internal tides that focus and break in the canyons. Internal tides cause water to slosh up and down a canyon axis (Hotchkiss and Wunsch, 1982), resuspending sediment and advecting it seaward along isopycnals as an intermediate (within the water column) nepheloid layer (Gardner, 1989a, 1989b; Puig et al., 2014). Such events carry orders of magnitude less PM per event than do turbidity currents, but they can occur with orders of magnitude greater frequency, occurring even daily from tidal oscillations and nonlinear dynamics of internal waves impinging on slopes (Cacchione and Wunsch, 1974; Cacchione et al., 2002). The PM is mixed with slope water and is rarely observed by optical measurements far from the canyon mouth (Gardner, 1989a), so it is likely to contribute little to benthic nepheloid layers far from continental margins.

2.4. PM advected from surrounding features

Benthic nepheloid layers begin at the nephel minimum (Fig. 1 insert) and usually extend to the seafloor. Particle concentrations at the minimum are typically ~10–15 μg l^{-1} (Brewer et al., 1976), and PM concentrations > 20–30 μg l^{-1} are usually confined to within ~100 mab, which is consistent with the typical thickness of the bottom mixed layer (BML) as defined by uniform potential temperature. Armi and D'Asaro (1980), using data from moored current meters and thermistor chains, found that BML thickness varied from 0 to 60 m over a three-month period in the western North Atlantic, with 20–30 m thicknesses being most common. Other studies by Armi and Millard (1976) reported BMLs varying from 10 m to 100 m depending on bottom topography, slope, and current speeds.

On the other hand, Biscaye and Eittreim (1977), Gardner et al. (1985a), Isley et al. (1990), Klein and Mittelstaedt (1992), and Puig et al. (2013b) have reported nepheloid layers as much as 1000–1500 m thick where there is no evidence from other properties (e.g. T, S) for vertical mixing of that magnitude. Could eddy diffusion gradually mix PM that high? Eittreim and Ewing (1972) calculated the eddy diffusivity necessary to explain diffusional mixing up to 1000–1500 mab; for clay particles of various sizes and settling velocities the eddy diffusivity would have to be 100 cm^2 s^{-1}, two orders of magnitude greater than vertical diffusivities of 1 cm^2 s^{-1} calculated for most of the deep ocean (Bell, 1974). The presence of kilometer-thick nepheloid layers can be better explained by horizontal advection and mixing of sediment eroded from surrounding topographic features such as seamounts, ridges and continental margins (Armi and Millard, 1976; Johnson and Lonsdale, 1976; Armi, 1978; McCave, 1986). Turnewitsch et al. (2013) pointed out that seafloor features with topographic relief > 100 m are common and can interrupt flow to cause local mixing and sediment resuspension. Thus, sediment can be resuspended from the seafloor on such features (e.g. New England Seamount Chain), then advected and mixed along isopycnals above deeper waters to create a thick nepheloid layer.

2.5. Seafloor erosion and PM transport by abyssal currents

For sediments to be eroded, current speeds must exceed the critical bed shear stress for the local sediment type (e.g., Sternberg, 1971). The required shear stress varies with grain-size distribution and shape, particle composition, cohesion, history of deposition and consolidation, and bottom microtopography. In terms of current speed 1 mab, velocities of 6–8 cm s^{-1} have moved low-density aggregates of phytodetritus (mm to cm in size) in both field (Lampitt, 1985) and flume studies (Beaulieu, 2003). Sediment in the non-cohesive, silt-size range requires speeds of 10–15 cm s^{-1} for erosion (McCave and Hall, 2006). From a compilation of theoretical, flume, and field measurements for critical erosion velocities of bioturbated silty sediments, the predicted resuspension of fine silt could be expected at free-stream velocities (i.e., above the bottom boundary layer) as low as 11–12 cm s^{-1} with sand being resuspended at 25–30 cm s^{-1} (Gardner, 1989a). Considering these data, minimum current speeds needed to erode sediments that have the grain sizes documented in PM samples are likely in the range of 10–20 cm s^{-1}.

Once resuspended, PM can be maintained in the water column at velocities much lower than are required to erode seafloor sediments (Partheniades, 1965; Krone, 1993). McCave (1986) estimated that it could take up to years for individual clay-size particles to settle out in

still water. It is more likely that particles are removed from the water column by aggregating with other particles (McCave, 1984). In addition, when filter feeding and excretion by benthic zooplankton are considered (Wishner and Gowing, 1992), the residence time of PM in the nepheloid layer may be only weeks to months as estimated from sediment trap data (Gardner et al., 1985b). Nonetheless, this is sufficient time for PM to be transported long distances, thus creating a persistent nepheloid layer.

As will be discussed in this paper, benthic storms are generally coincident with current speeds in excess of ~20 cm s^{-1} (Hollister and McCave, 1984), and they generate pronounced increases in the concentration of PM in the BML. On the other hand, high PM concentrations are sometimes found to correlate with low current speeds; this indicates either advection from a distal event or slowing of currents following a local event. We refer to these occurrences as 'storm tails'. Differentiating benthic storms from storm tails at a given location requires that both current speed and PM concentrations be measured. High current speeds don't guarantee high PM. The local seafloor could be denuded - stripped of sediment susceptible to erosion (i.e., 'stress hardened', Hollister and McCave, 1984) by the ambient current or by a preceding storm. The best way to document local erosion is by visual (e.g., photographic) observation; however, visual verification may be difficult considering that a significant increase in PM concentrations in the nepheloid layer can be caused by erosion of only a fraction of a millimeter of seafloor sediment.

3. Methods

3.1. Instruments and calibrations

The data that we report here are from four deployments of a BOM tripod system (Supplementary Fig. S1), four moorings with a near-bottom LTN that made time-series measurements at one- to four-hour intervals, and one mooring with a transmissometer (Figs. 2 to 5, Table 1). The BOM configuration consisted of a tripod with a 35 mm film camera and strobe light to record seafloor conditions over 0.23 to 1.33 m^2, a horizontally positioned LTN attached to the tripod frame at 0.6–1.2 mab, and an Aanderaa current meter tethered at 3.5–6.7 mab. On moorings, the LTN was mounted horizontally within a vertical array containing other instruments. The LTN used a white strobe-light source and single-frame film advance (Gardner and Sullivan, 1981) providing discrete snapshot measurements of E/E_D.

Biscaye and Eittreim (1977) showed log E/E_D to be linearly correlated with particle concentration on a log-log plot up to at least 300 μg l^{-1} (their maximum sampled concentration) using the equation:

$$\log(PM) = 1.192 * \log(E/E_D) + 0.134.$$

(Note that the Biscaye and Eittreim (1977) paper had a typographical error and the above equation is the correct one.) Biscaye and Eittreim (1977) used this equation to convert E/E_D to particle concentration and calculate the total integrated nepheloid layer PM load (μg cm^{-2}) at each station.

Regressions between E/E_D from the profiling nephelometer and PM concentration were calculated by Gardner et al. (1985a) for the HEBBLE program. Several HEBBLE samples exceeded 2000 μg l^{-1} (the maximum benthic particle concentration measured by filtration was 12,700 μg l^{-1}, i.e., visually turbid water), much higher than maximum concentrations of ~300 μg l^{-1} in other studies (Biscaye and Eittreim, 1977; Richardson, 1987; Richardson et al., 1987). Above concentrations of about 200 μg l^{-1} in the HEBBLE region, the relationship between particle concentration and E/E_D became non-linear and was best fit with a quadratic equation:

$$PM = 0.026(E/E_D)^2 + 1.08(E/E_D) + 12.1,$$

which yields slightly lower concentrations in the ~30–200 μg l^{-1} range and much higher concentrations in the <25 μg l^{-1} range than the linear equation of Biscaye and Eittreim (1977) Most of the nephelometer profiles in Fig. 1, collected over a 20-year period, yielded concentrations that were <200 μg l^{-1}; thus for this figure (and Figs. 6 and 15) we used the Biscaye and Eittreim (1977) equation to convert E/E_D to particle concentration and to calculate the excess PM load (μg cm^{-2}). However, because E/E_D peaks in LTN records often greatly exceeded values of 200 μg l^{-1}, plots of LTN data are scaled using the quadratic equation to indicate PM concentration, with the exceptions of BOM D and BOM T (Fig. 2); for those records we used the Biscaye and Eittreim (1977) equation which better represents the observed, consistently low PM concentrations.

Transmissometers were incorporated in deployments of BOM H and mooring CMME-6, ~16 km southeast of BOM S ('C6' in Fig. 1). We include here the latter record, which was obtained using a 25-cm Sea Tech transmissometer that measured beam attenuation (c_p, another proxy for particle concentrations) (Boss et al., 2014).

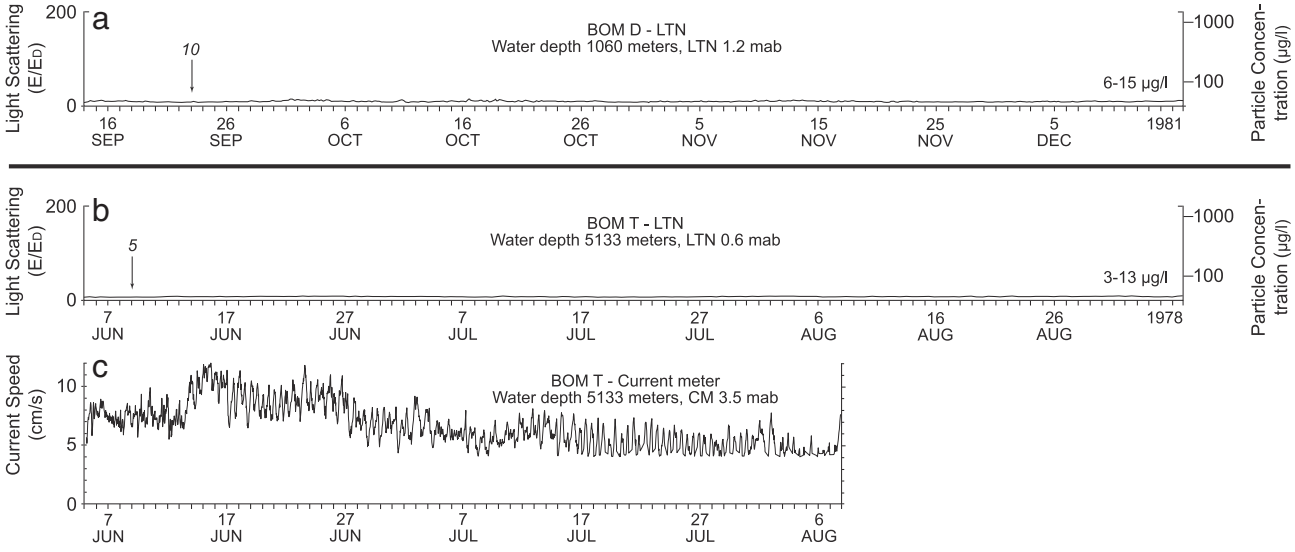

Fig. 2. Representative segments of time-series LTN records of E/E_D (left axis) and PM concentration (right axis) in areas of low EKE. a) BOM D and b) BOM T in the western North Atlantic. c) Current-meter record for BOM T. See Fig. 1 for site locations. The time, E/E_D and PM concentration scales for these plots are the same as in Figs. 3 and 4. The PM scale is based on calibrations of Biscaye and Eittreim (1977). The times of photographs taken on day 10 of BOM D and on day 5 of BOM T are shown with arrows in a) and b); the photographs are shown in Fig. 12e and f.

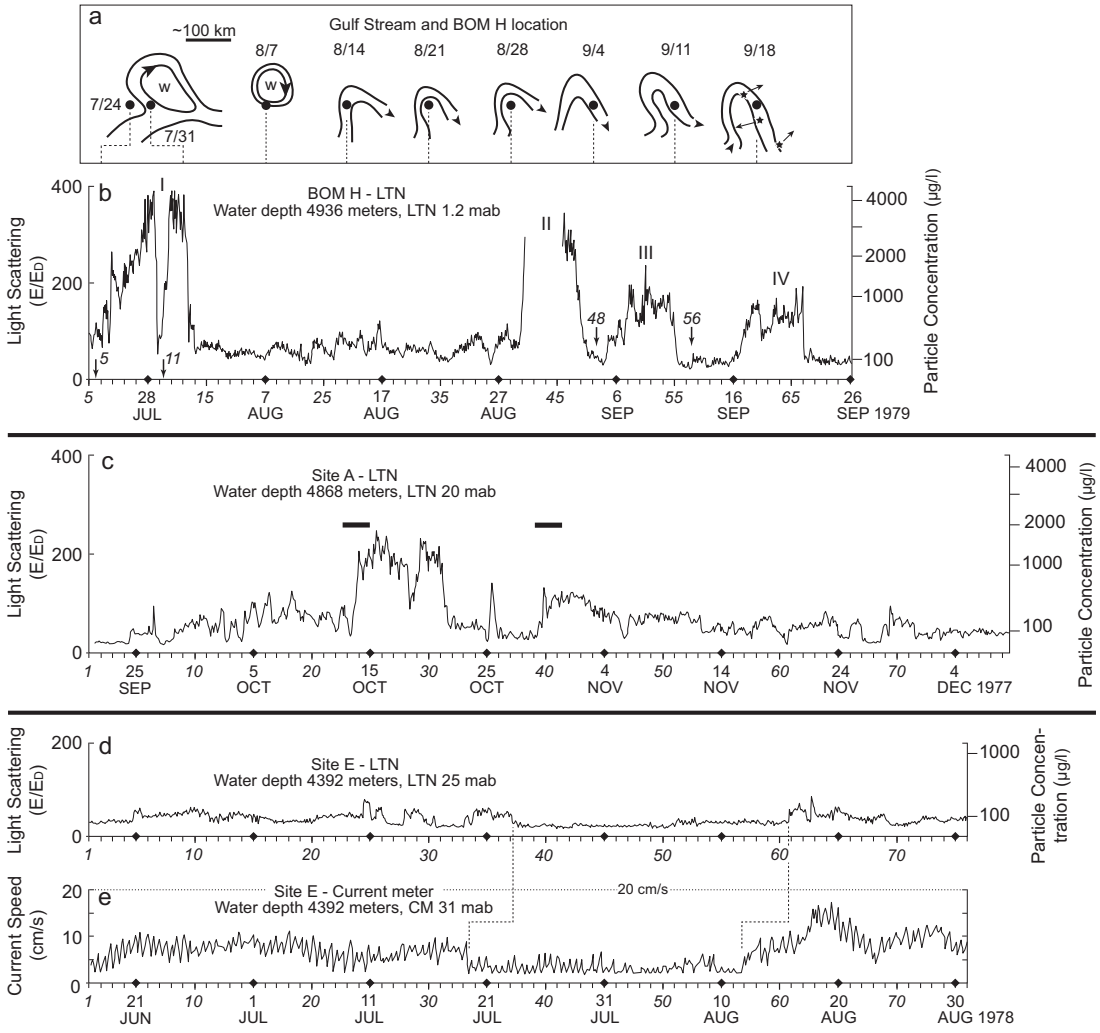

Fig. 3. Time-series records for three sites in areas of moderate to high EKE in the western North Atlantic. In the LTN records of b) to d), the time, E/E_D (left axis) and PM concentration (right axis) scales are the same as in Figs. 2 and 4. Italic numbers on time axes indicate the beginning of each day into the deployment. Site locations are in Fig. 1. a, b) BOM H on the Nova Scotian lower continental rise (camera and LTN were started on deck ~5days before deployment). In a), the position of the Gulf Stream and its rings is shown with respect to the location of BOM H (black dot) at specified times (dotted lines and month/day). At 9/18, the stars and arrows show mean current directions at current-meter moorings set in the area during the last two weeks of the BOM H deployment (see text). b) The LTN record of BOM H, with benthic storms numbered I–IV. Peak PM values during storm II were beyond the instrument's range. Arrows and numbers at the bottom indicate deployment-day times of bottom photographs shown in Fig. 12a–d. c) LTN record at mooring A on the northwest Bermuda Rise, from Gardner and Sullivan (1981). Horizontal bars indicate times of passage of a hurricane and a subsequent tropical storm. d) LTN record at mooring E on the northeast Bermuda Rise, and e) mooring E current-meter record, both from Laine et al. (1994). In e), current speed of 20 cm s^{-1} is marked by a horizontal dotted line for reference. The other dotted lines in d) and e) indicate a ~4-day lag time between current and PM events.

Time-lapse bottom photographs from BOM S and BOM D were made into videos so that processes of seafloor modification could be observed. These videos are available in the Supplementary material (S4, S5).

3.2. Hydrographic features

We evaluated our measurements in the context of their location relative to the Gulf Stream (GS), its meanders and rings, and the presence of shelf, slope, and Sargasso Sea waters determined using 1) Ocean Frontal Analysis of the US Naval Oceanographic Office (Code 9100 (3710)), 2) Gulf Stream Analysis produced by NOAA-NESS-EPG using NOAA-5 VHRR satellite data, and 3) Oceanographic Analysis of the National Weather Service using the National Earth Satellite Service. Hand-contoured maps of all these were usually published weekly, which limits the temporal resolution of surface hydrographic features.

To examine the relationship of our measurements to surface EKE, we used the maps of Dixon et al. (2011) and Delworth et al. (2012). They calculated EKE using instantaneous values of near-surface currents calculated from sea surface height (SSH) fields every seven days and assuming geostrophy. Eddy velocities were computed as deviations from a five-year mean of currents, from which EKE was calculated. EKE is the energy associated with temporal deviations from the mean energy of the fluid flow. It is defined as $EKE = 0.5 * (\overline{u'^2} + \overline{v'^2})$, where u′ and v′ are standard deviations from the mean current velocity in the east-west and north-south directions, respectively. Mean kinetic energy is derived from a similar equation, but uses u and v rather than u′ and v′.

4. Results

4.1. Overview of LTN time-series

Most LTN time-series records show large variations in E/E_D and thus in PM concentrations. The records are divided into two groups: 1) low background concentrations (<20 µg l^{-1}) and small temporal variability (Fig. 2), and 2) high background PM concentrations (20–140 µg l^{-1}) and large temporal variability (Figs. 3–5). To facilitate comparison among the LTN records, data for deployments in Figs. 3 and 4 are

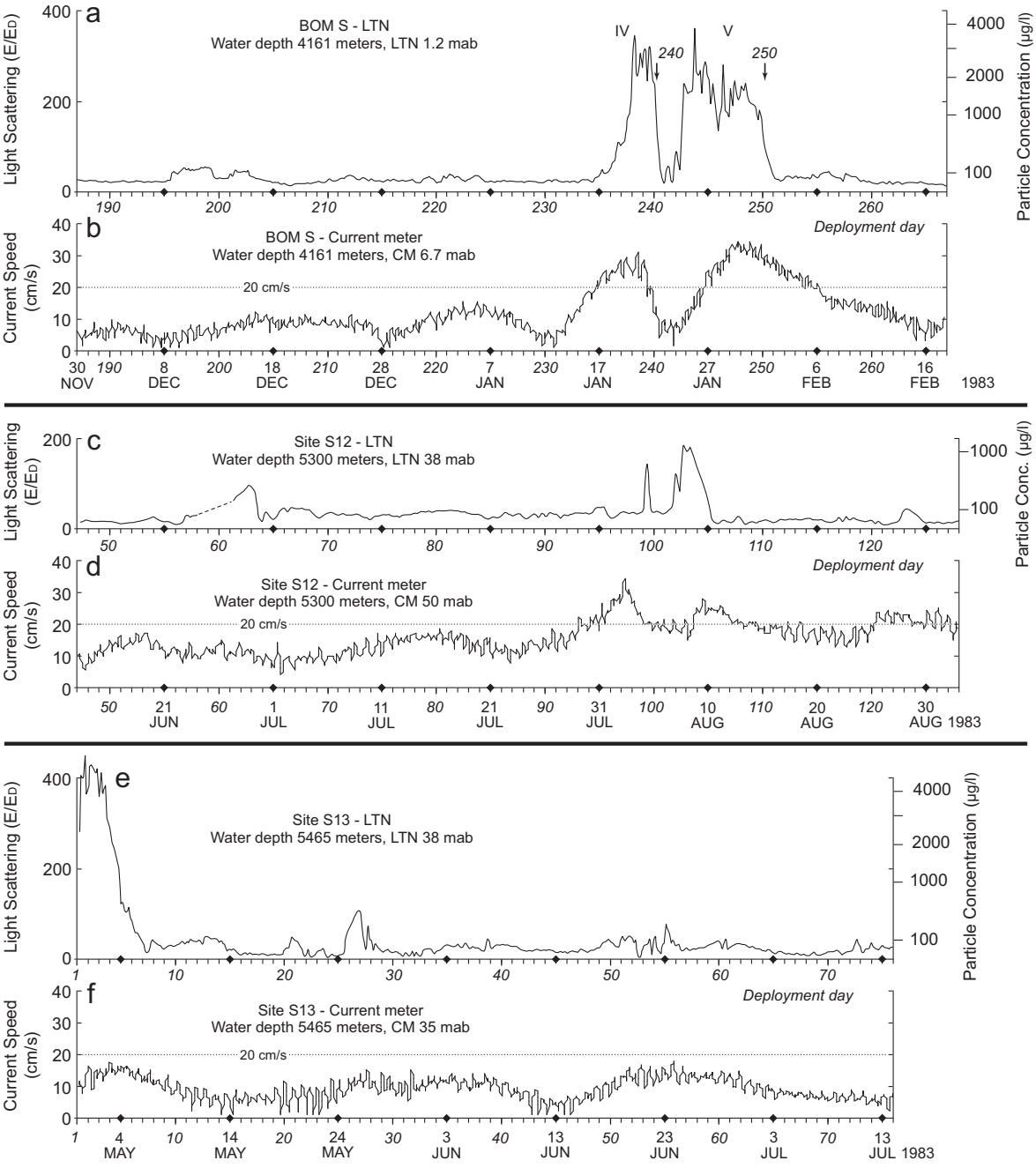

Fig. 4. Time-series records of E/E_D (left axis) and PM concentration (right axis) in areas of moderate to high EKE in the western North Atlantic, together with current-meter records. Scales on the LTN records (a, c and e) and other labels are the same as in Fig. 3. a) LTN record of BOM S on the central continental rise east of Cape Hatteras. Only a segment of the record is shown here (see Table 1); the full record is in Fig. 5a–e. Roman numerals IV and V identify benthic storms, and arrows with italic numbers indicate deployment-day times of bottom photographs shown in Fig. 11. b) Current-meter record at BOM S. c) LTN record at mooring S12 on the lower continental rise. Only part of the record is shown (see Table 1); the full record is in Fig. S2. d) The corresponding current-meter record at S12. e) The complete LTN record at S13 on the northwestern Hatteras Abyssal Plain. f) The corresponding current-meter record at S13. Both the LTN record and the longer-term current record at S13 are shown in Fig. S3.

displayed using the same scales for time (x-axis), light scattering (E/E_D; y-axis left side), and PM concentration (µg l^{-1}; y-axis right side), using the quadratic equation of Gardner et al. (1985a). The BOM D and BOM T records in Fig. 2, with PM calculated using the Biscaye and Eittreim (1977) equation, are segments of the full records but are representative of low light scattering observed throughout the deployments (Table 1). To keep horizontal time scales the same, only segments of the BOM S and S12/S13 LTN records are shown in Fig. 4; at different scales, the full LTN record of BOM S is shown in Fig. 5 and the full records of S12 and S13 are in Supplementary Figs. S2 and S3. Information and statistics in Table 1 represent the entire dataset at each site.

Fig. 6 shows mean E/E_D and standard deviation of E/E_D at measurement sites (see also Table 1) together with isopleths of abyssal EKE (green dashed lines) and excess PM load (solid red lines from Fig. 1). Sites with the highest abyssal EKE generally have the highest mean E/E_D and standard deviation (Table 1), suggesting that the greater the energy near the seafloor, the greater is the likelihood of episodic sediment resuspension events (benthic storms).

We calculated abyssal EKE from current-meter records where those data were available (BOM S, BOM T, and moorings S12, S13 and E; Table 1) to graphically compare abyssal EKE and standard deviation of E/E_D (Fig. 7). Current-meter data at S12 and S13 were Lanczos low-

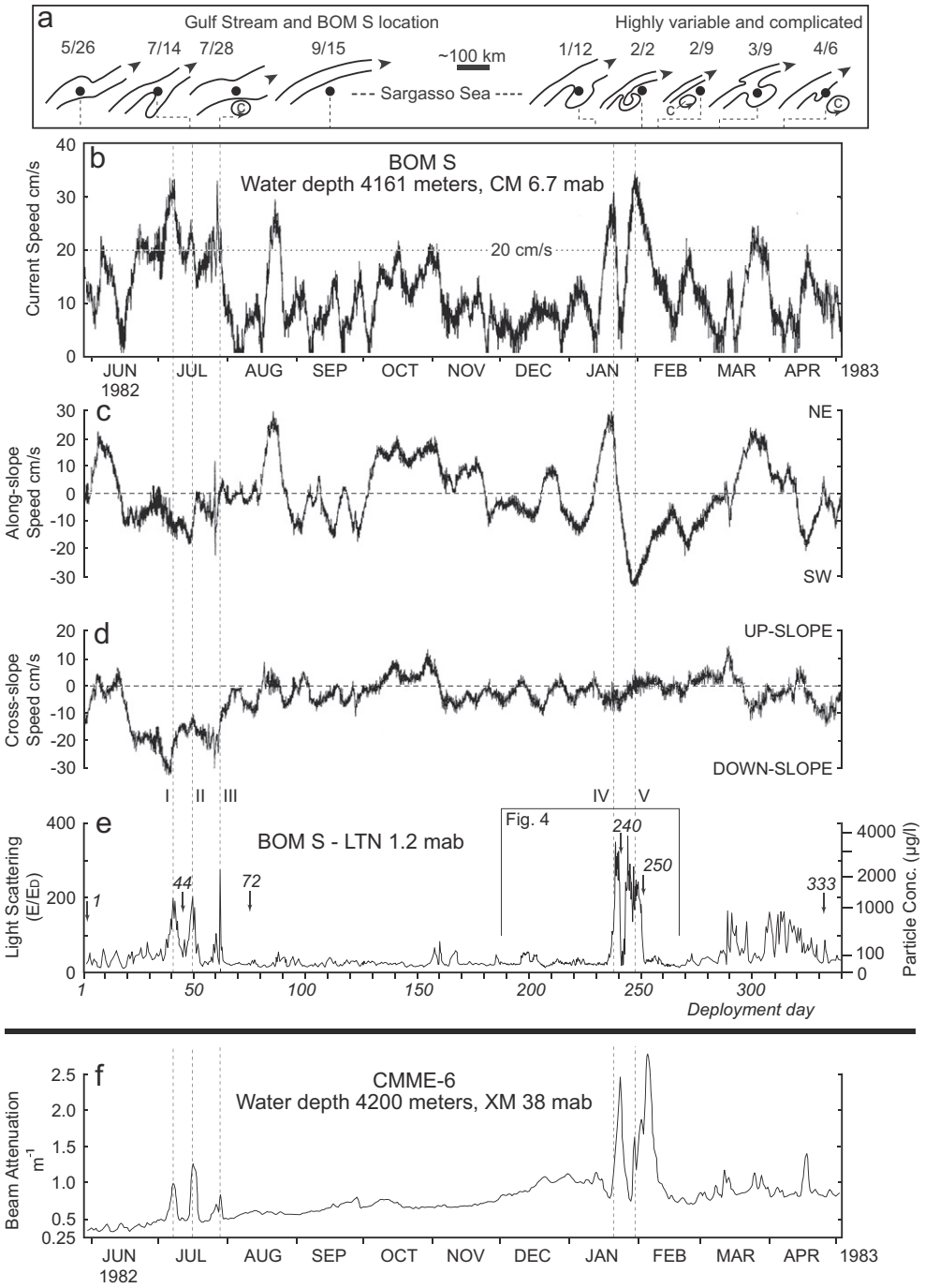

Fig. 5. Complete time-series records at BOM S and corresponding beam-attenuation record at mooring CMME-6, ~16 km southeast of the BOM. Scales of these records differ from those in prior figures, but annotations are the same. a) Gulf Stream position with respect to BOM S and CMME-6, as explained in Fig. 3 caption. At this scale, the black dot encompasses both BOM S and CMME-6. The BOM S record shows b) current speed, c, d) along-slope and cross-slope current components, and e) E/E_D and PM concentration from the LTN. In panel e), Roman numerals identify benthic storms I–V and arrows with italic numbers indicate deployment-day times of bottom photographs shown in Fig. 11. See Fig. 4a, b for a detailed view of benthic storms IV and V at BOM S. f) Beam attenuation from a transmissometer attached 38 mab at CMME-6. Vertical dotted lines through the panels mark the timing of five benthic storms at BOM S.

pass filtered by Pillsbury et al. (1985) to remove tides before calculating abyssal EKE. Current speeds were not measured at mooring A, are not available for BOM D, and they are available for only the first two days at BOM H. For those sites, ranges of EKE were estimated from data and maps of Weatherly (1984) and Schmitz (1984). The resulting plot indicates that there is a strong correlation between abyssal EKE and standard deviation of E/E_D. One exception is S13, which has the second highest E/E_D of all observations (Fig. 4e), but is somewhat questionable. The high standard deviation of E/E_D at S13 is due to a 6-day period of high PM concentrations at the beginning of the record that was not associated with an unusually strong or fluctuating current. With this 6-day period removed (S13′ in Fig. 7), the data from this site agree closely with the trend from other sites.

4.2. Time-series observations at individual sites

4.2.1. BOM S and mooring CMME-6 – U.S. central continental rise

BOM S (Figs. 1, 4a, b, 5) was deployed as part of a Sandia National Laboratories project on the central to lowermost continental rise of the eastern United States (Gardner, 1986). It included an LTN, current

Table 1
Time series BOM and moored nephelometer, current meter and camera metadata; Listed in order of background (E/ED) intensity.

BOM/mooring				Nephelometer			Light scattering (E/ED)					Current meter		EKE	Bottom photos	Funding	References
Station	Lat. °N Lon. °W	Water depth (m)	Deploy Recover	m above bottom	No. of days sampled	Sampling interval (h)	Max.	Min.	Mean	Std. dev.	Back-ground μg l^{-1}	CM m above bottom	CM days	cm^2 s^{-2}	Days, interval		
BOM H	40.09° 62.40°	4936	7/24/79 9/26/79	1.2	65	1	389	14.5	104	±79	80–140	3.5	2	115[a]	65 days, 1 h	ONR	Gardner et al. (1985a)
A	35.68° 65.85°	4868	9/23/77 12/10/77	20	78	2	245	16.6	69	±44	80–140	–	–	75[a]	–	NSF	Gardner and Sullivan (1981)
BOM S	36.36° 71.60°	4161	5/29/82 5/3/83	1.2	340	4	363	12.9	46	±45	50–80	6.7	340	90	340 days, 4 h	Sandia	This paper
CMME-6	36.28° 71.46°	4200	5/28/82 5/3/83	38 Tr	–	–	–	–	–	–	–	40	340		–	Sandia	Pillsbury et al. (1984) This paper
S12	33.70° 71.03°	5300	4/28/83 9/8/84	38	214	4	182	3.7	25	±20	35–80	50	485	58	–	Sandia	This paper
E	33.08° 57.80°	4392	6/18/78 8/31/78	25	75	1	83	18.6	36	±11	35–60	31	75	10	–	ONR, NSF	Laine et al. (1994)
S13	32.77° 70.79°	5465	4/30/83 8/28/84	38	75	4	468	3.5	44	±76	20–50	35	485	35	–	Sandia	This paper
S13′ (with first 6 days removed)					69	4	107	3.5	26	±15	20–50			35	–	Sandia	This paper
BOM D	39.82° 70.78°	1060	9/15/81 7/19/82[b]	1.2	308	4	15	4.6	7.4	±1.4	6–15	–	–	2[a]	308 days, 4 h	DOE	This paper
BOM T	23.64° 68.43°	5133	6/6/78 11/20/78	0.6	168	2	6.8	3.3	4.6	±0.70	3–13	3.5	66	4	169 days, 4 h	ONR	This paper
				Total days	1323												

Tr = Transmissometer.
[a] Estimate of mean abyssal EKE comes from Fig. 6 map.
[b] Exact date uncertain.

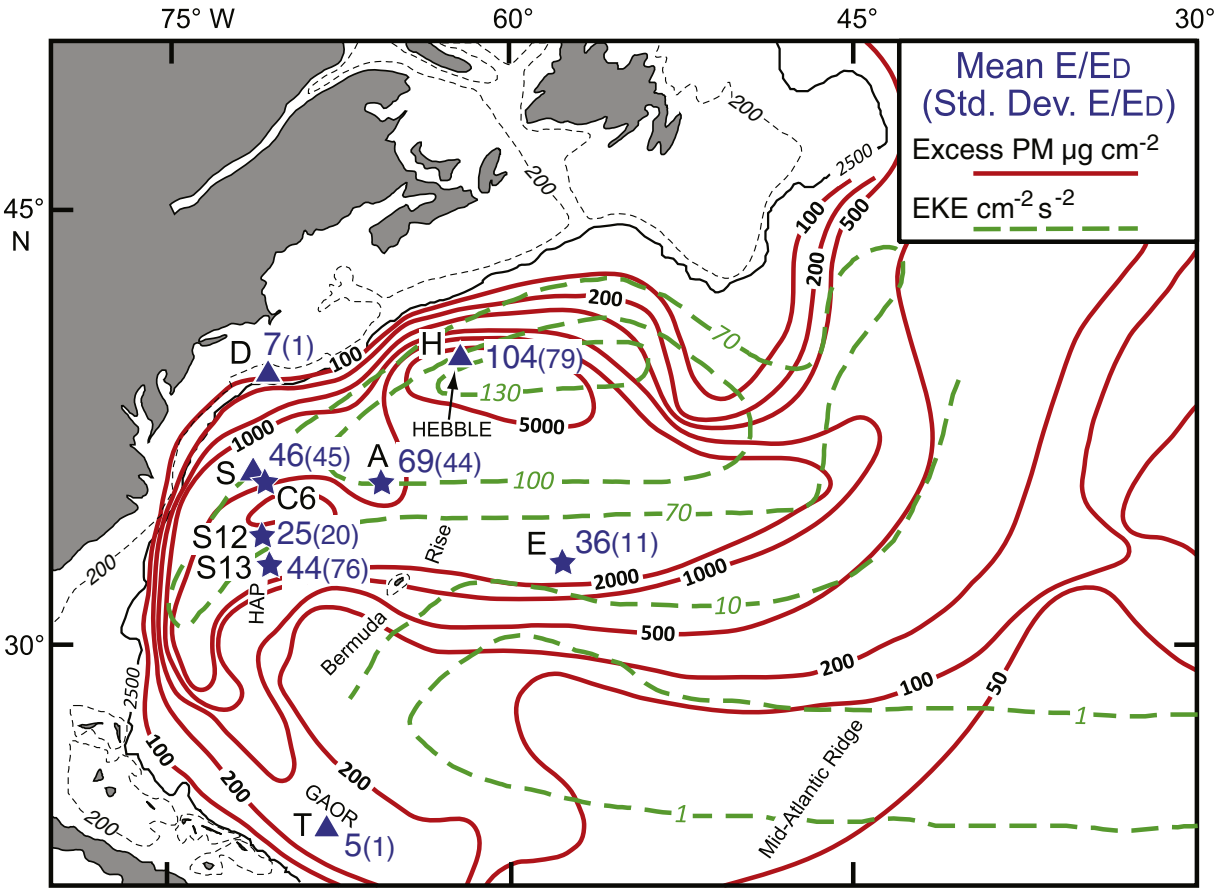

Fig. 6. Contours of excess PM load in the benthic nepheloid layer (red lines, in µg cm^{-2}) from Fig. 1, together with contours of abyssal EKE (dashed green lines, in cm^2 s^{-2}) combined from Schmitz (1984) and Weatherly (1984). Numbers at BOM and mooring locations indicate mean E/E_D and standard deviation of E/E_D (in parentheses) calculated from LTN time series. At BOM locations (D, H, S, T) the LTNs were about 1 mab and at mooring sites (A, S12, S13, E) they were 20–38 mab (Table 1). C6 is current-meter mooring CMME-6.

meter, and time-lapse bottom camera. Simultaneously with the BOM S record, currents were also recorded at four depths on mooring CMME-6 (Figs. 1 and 8) (Pillsbury et al., 1984). A Sea Tech transmissometer at 38 mab was close to the current meter at 40 mab at CMME-6 (Fig. 5f). Statistics and plots of the BOM S current-meter data are given by Pillsbury et al. (1984, 1985) and Gardner (1986).

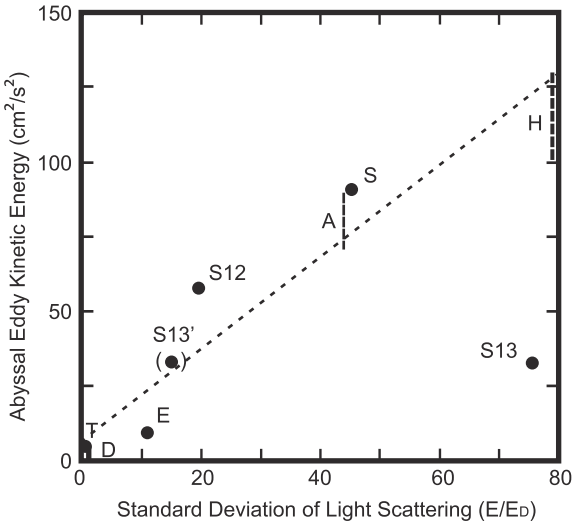

Fig. 7. Abyssal EKE versus variability in light scattering (standard deviation of E/E_D) at LTN measurement sites. The range of EKE for mooring A, BOM D and BOM H (bold dashed lines) is from contour maps of Schmitz (1984) and Weatherly (1984). The light dashed line shows a linear regression fit to the data using S13′ (not S13), which excludes a 6-day high-PM event at the beginning of S13, and using the mid-point estimates of EKE for A and H. See text for details.

The BOM S nephelometer, current meter, and camera system functioned perfectly for the entire deployment (Figs. 4a, b and 5) (Gardner, 1986). Photographs of the seafloor and LTN measurements of light scattering were taken every 4 h.

Measured currents during the first two months of the BOM S deployment were predominantly cross-slope, perpendicular to the regional contours, at up to 30 cm s^{-1} (Figs. 5, 8e and 9). During most of the remaining time the flow was oriented along the regional contours, oscillating between northeast and southwest with 1- to 2-month periods and with speeds similar to those of the earlier cross-slope flow. The mean current speed during the deployment was 12.2 cm s^{-1}, and the mean velocity was 3.85 cm s^{-1} to the southeast.

Spectral analysis of unfiltered along-slope and cross-slope components of currents at 7 mab (Fig. 10a, b) shows energy peaks near diurnal/inertial and semi-diurnal frequencies. The mean flow, however, is much stronger than the tidal variations, as evidenced by the lack of significant variations on tidal time scales in the unfiltered time-series plots of total current, along-slope, and cross-slope current speeds (Fig. 5b–d).

CMME-6 current meters were deployed at 1250, 2800, 3400 and 4160 m in a water depth of 4200 m (Fig. 8a–d) (Pillsbury et al., 1984). Currents at 2800, 3400 and 4160 m were very coherent in speed and direction but they were less coherent with currents at 1250 m. Spectral analysis of unfiltered currents (hourly) showed nearly equal energy at diurnal and semidiurnal frequencies at 4160 m (Pillsbury et al., 1984). CMME-6 currents at 4160 m (40 mab) and BOM S currents at 4154 m (6.7 mab) were highly coherent (squared coherence > 0.9; Pillsbury et al., 1984).

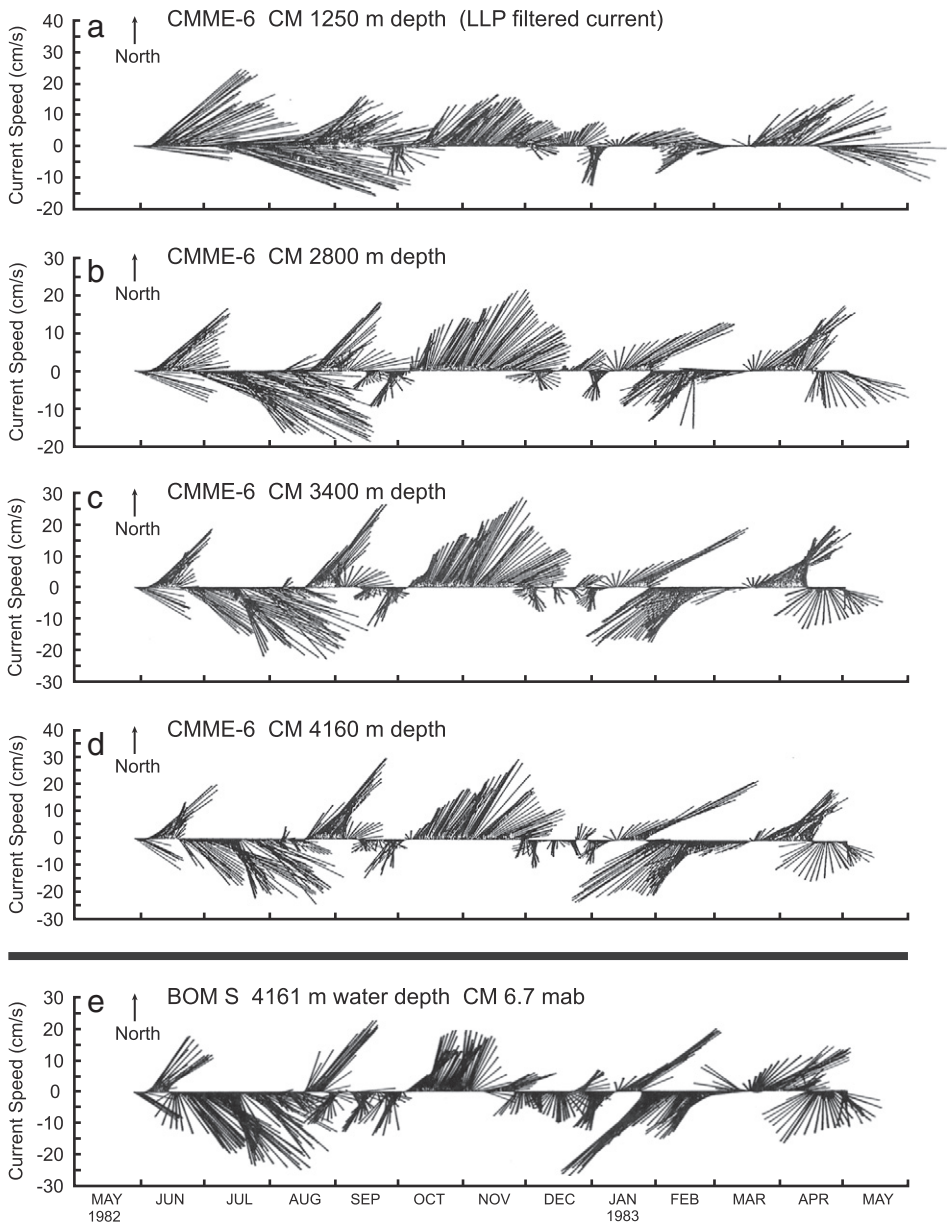

Fig. 8. Stick diagrams of currents throughout the water column at mooring CMME-6, ~16 km southeast of BOM S (a–d), and at BOM S (e). The diagrams were made from Lanczos low-pass filtered u and v current components, and for clarity only two sticks per day are plotted (Pillsbury et al., 1984). Note that vertical scales differ slightly.

The LTN at BOM S was located 1.2 mab. Background PM concentration based on calibrations of the nephelometer (Gardner et al., 1985a) generally ranged from 50 to 80 μg l^{-1}, with a minimum of 25 μg l^{-1} (Fig. 5e). Spectral analysis of the LTN record revealed no statistically significant E/E_D peaks near tidal frequencies (Fig. 10c).

There were five distinct benthic storms between July 1982 and February 1983 (Fig. 5e, f). Increases in PM from the LTN record at BOM S coincided or were slightly out of phase with increases in transmissometer beam attenuation at CMME-6. Subsequently, during mid-March to mid-April 1983 when a cold-core ring was detaching from the GS, there were also episodes of variably elevated PM at both locations, but these show poor correlation with one another, with locally measured currents, and with changes in seafloor texture photographed at BOM S.

Time-lapse bottom photographs of a 0.61 × 0.46 m area were taken every 4 h throughout the 340-day BOM S deployment (Fig. 11 and Supplemental Video S4). The seafloor appeared to consist of fine-grained sediment, but no sediment samples were obtained. The micro- and macro-scale morphology of the seafloor changed dramatically over the course of a year. Some of the changes were gradual, but most of the changes occurred over the course of a few days and sometimes within a few hours.

The compass was in camera view throughout the deployment, and bedform indicators of sediment transport correlated well with measured current directions. Resuspended sediment totally obscured the seafloor during storms III to V. The character and timing of fluctuations in measured parameters coincided in all the storms: faster currents, increased LTN values, and sediment movement and/or turbidity observed in bottom photographs.

The photographic record showed occasional benthic epifauna including 13 frames with holothurians, five with ophiuroids, a gastropod, numerous tracks in the sediment, and a fish shadow. Sometimes there were no visible seafloor changes for a day or two and at other times tracks were added throughout the field of view during the 4 h between photographs. Occasionally a drifting clump of Sargassum was caught on the camera compass and left marks on the sediment surface. The perseverance of burrowing animals was demonstrated by re-excavation of

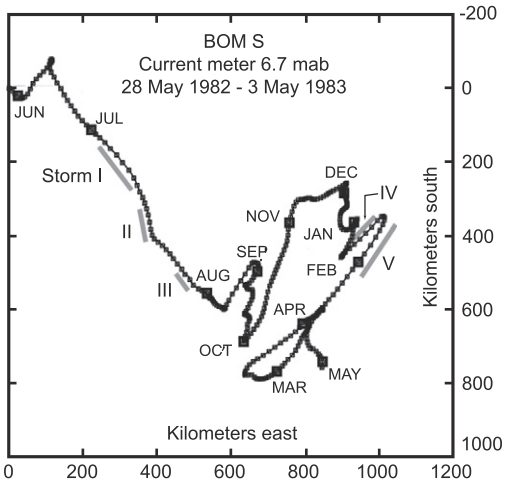

Fig. 9. Progressive vector diagram of currents measured 6.7 mab at BOM S during its 11-month deployment. Initial flow was mostly perpendicular to regional bathymetric contours for ~40 days and thereafter tended to fluctuate between NE and SW, parallel to contours. Large squares indicate the first day of each month and small squares are daily marks. Gray bars show the times of benthic storms, identified with Roman numerals I–V.

the animals' burrows after they were filled with sediment during benthic storms. Sediment movement along the bottom sometimes occurred between major storms (e.g. mid-late August and March–April), but most movement was during very short periods of fast currents.

4.2.2. Moorings S12 and S13– U.S. lower continental rise and Hatteras Abyssal Plain

These moorings were also part of the Sandia National Laboratories project, and they included both LTNs and current meters (Table 1). Statistics and plots of the current-meter data are given by Pillsbury et al. (1984, 1985) and Gardner (1986). Isley et al. (1990) reported current measurements and changes in the nepheloid layer (percent changes in transmissometer beam attenuation) during the preceding two years at S13 and at a site ~ 100 km southwest of S13 during the year before our measurements.

Measured currents at S12 (Figs. 1, 4d, and S2) had a maximum speed of 35 cm s^{-1} and a mean of 9.8 cm s^{-1} during 16 months of deployment. At S13 the maximum and mean currents were 20 cm s^{-1} and 6.7 cm s^{-1} during the same time (Figs. 4f and S3). Spectral analysis of the current meter records for both S12 and S13 shows peaks at diurnal, inertial and semidiurnal tidal periods, similar to BOM S (Fig. 10a, b). Also similar to BOM S currents, the mean flow was much stronger than the tidal variations (Figs. 4d, f, S2c, and S3c).

The LTNs at S12 (Figs. 4c, S2) and S13 (Figs. 4e, S3) collected time-series data at four-hour intervals. At S13, the LTN provided data for only the first two and a half months of the deployment. The S12 and S13 records (100 km apart) overlap in time from 15 June to 15 July.

Evidence of benthic storms was found at both sites (Fig. 4c, e). The lowest background PM concentrations at these sites were slightly lower than the earlier record at BOM S (Table 1), but the LTNs on the moorings were at 38 mab compared with 1.2 mab at BOM S, so lower concentrations are to be expected. The S12 LTN data show a correlation with increased current speed in late October and possibly mid-September (Fig. S2), but LTN events in late June and August were uncorrelated or distinctly out of phase, respectively, with current speeds (Fig. 4c, d). The 2.5-month LTN record at S13 registered extremely high light-scattering values at the beginning of the deployment (Fig. 4e) although the currents during this event were only about 10–15 cm s^{-1}. Overall, there is no clear correlation of light scattering with currents (Figs. 4e, f and S2). Spectral analysis of the LTN records at both S12 and S13 shows no tidal peaks, similar to the LTN record at BOM S.

4.2.3. BOM H - Nova Scotia lower continental rise, HEBBLE area

BOM H was deployed with an LTN, current meter, and time-lapse camera (Figs. 1 and 3a, b; Table 1) as part of the HEBBLE study on the lower continental rise south of Nova Scotia (Gardner et al., 1985a, 1986).

The current meter recorded data for only two days (mean speed 5 cm s^{-1}) before it flooded. However, Richardson et al. (1981) measured bottom currents 50 mab in the area for two weeks at seven sites between 4200 m and 5100 m water depth (Fig. 3a, right side). Mean current speeds increased from 8 cm s^{-1} at 4200 m to 32 cm s^{-1} at 5000 m, but there was significant variability, including maximum speeds of 73 cm s^{-1}. Currents at 4770 m and 5076 m (200 km apart) were moving northeast at ~20 cm s^{-1} while at the same time the current between those two sites was moving southwest at >60 cm s^{-1}, indicating that the bottom flows in the region were highly variable in space and time.

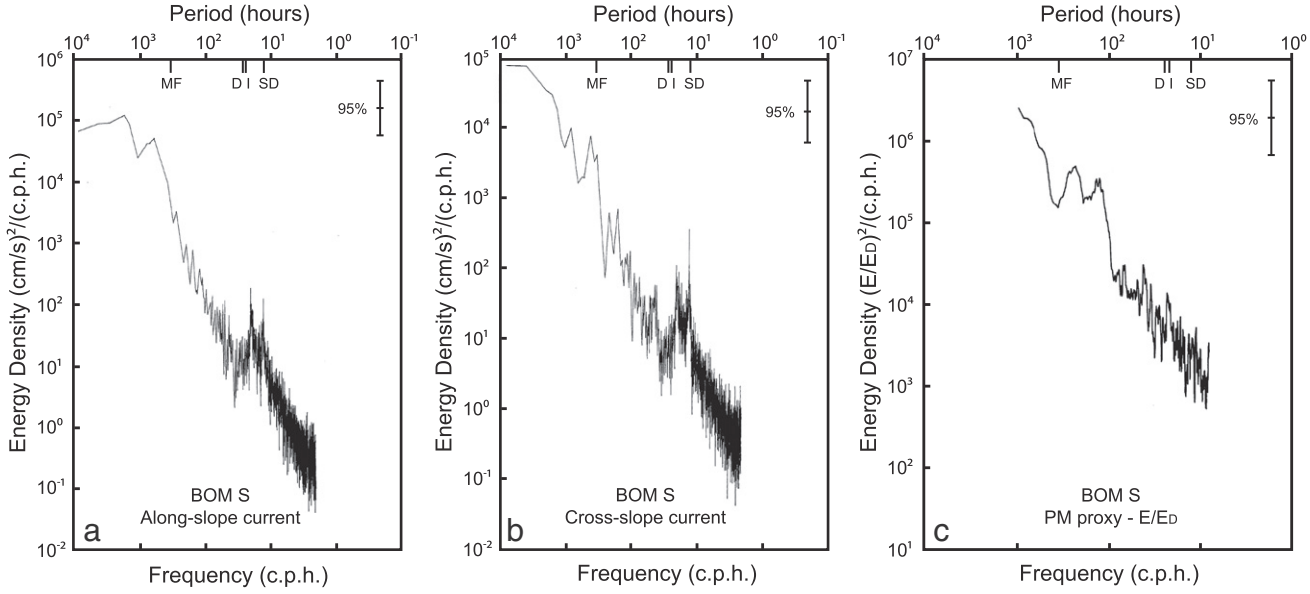

Fig. 10. Power spectra of unfiltered (a) along-slope and (b) cross-slope current speeds at BOM S. c) Power spectra of E/E_D at BOM S. Tidal periods of semi-diurnal (SD), diurnal (D), inertial (I) and mean fortnightly (MF) tides are indicated. The 95% confidence intervals are shown for the long-wavelength periods. Frequency is cycles per hour.

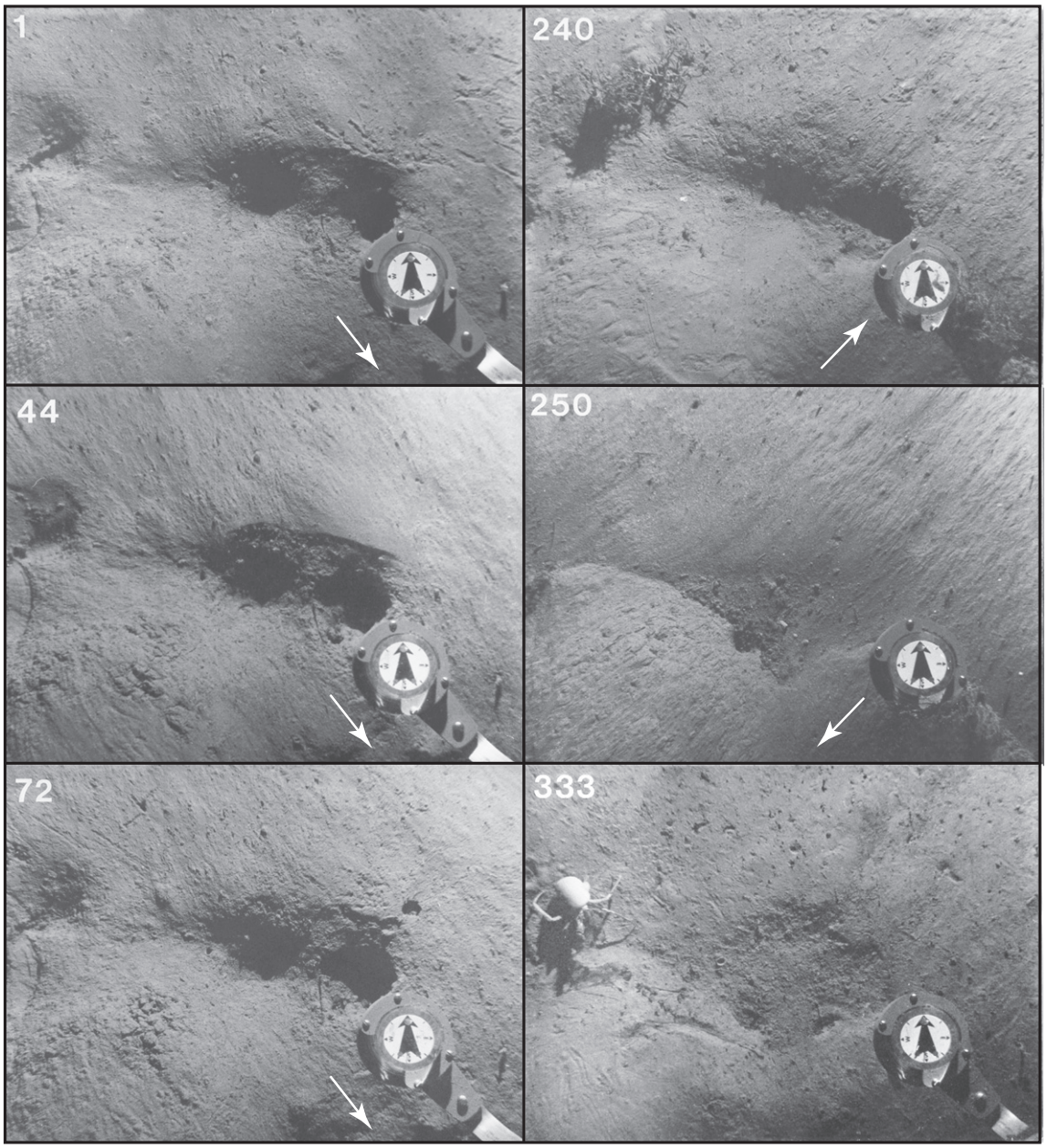

Fig. 11. Bottom photographs taken from time-lapse series at BOM S. Numbers are deployment-day dates and are marked on the E/E_D records in Figs. 4a and 5e. The imaged area in each frame is about 61 by 46 cm. Arrows indicate direction of most recent current that was strong enough to erode or reshape the seafloor, as indicated by seafloor striations and tool marks.

LTN data (Fig. 3b) were recorded hourly and evaluated by Gardner et al. (1985a). The maximum light scattering was almost double that recorded at mooring A, which was previously the maximum PM measured in the deep ocean (we note, however, that the LTN at mooring A was 20 mab compared with only 1.2 mab at BOM H). Four storm periods (I–IV) at BOM H were identified based on elevated LTN measurements (PM concentration > 1000 μg l^{-1}), with lower background concentrations (80–140 μg l^{-1}) recorded between storms. During two of the storms (I and II), peak PM concentrations exceeded 4000 μg l^{-1}.

Time-lapse bottom photographs of a 1.06 × 1.25 m area were obtained hourly during the entire deployment (Fig. 12a–d), but high PM concentrations reduced image clarity compared to other sites. A compass attached to the BOM was not in the field of view so current direction cannot be interpreted. The photographs show significant and remarkably rapid modification of the seafloor at sub-centimeter scales by both currents and biological processes over periods of hours to weeks. During benthic storms the seafloor was partially to totally obscured by clouds of resuspended PM. Surface samples from cores in this area indicate that the sediment is sandy clayey silt (sand:silt:clay = 16 ± 7%:44 ± 14%:35 ± 2%; B. Tucholke, unpublished data). A zone rich in clay (>40%) occurs between 4000 and 4800 m, and the silt/clay ratio increases steadily with water depth between 4000 and 5100 m (Driscoll et al., 1985), suggesting increased winnowing of clay with increasing water depth.

4.2.4. Mooring A - northwest Bermuda Rise

Mooring A was located at the juncture of the northwestern Bermuda Rise and the lower continental rise (Fig. 1). The LTN (Fig. 3c, Table 1) was attached 20 mab to a sediment-trap mooring (no current meters) and it provided the first evidence of what the authors termed "benthic storms" (Gardner and Sullivan, 1981). The LTN recorded at 2-hour intervals and showed a nearly 20-fold increase in PM concentration that coincided with the nearby passage (40 km) of Hurricane Evelyn in mid-October. The increased PM concentration lasted about one week. A

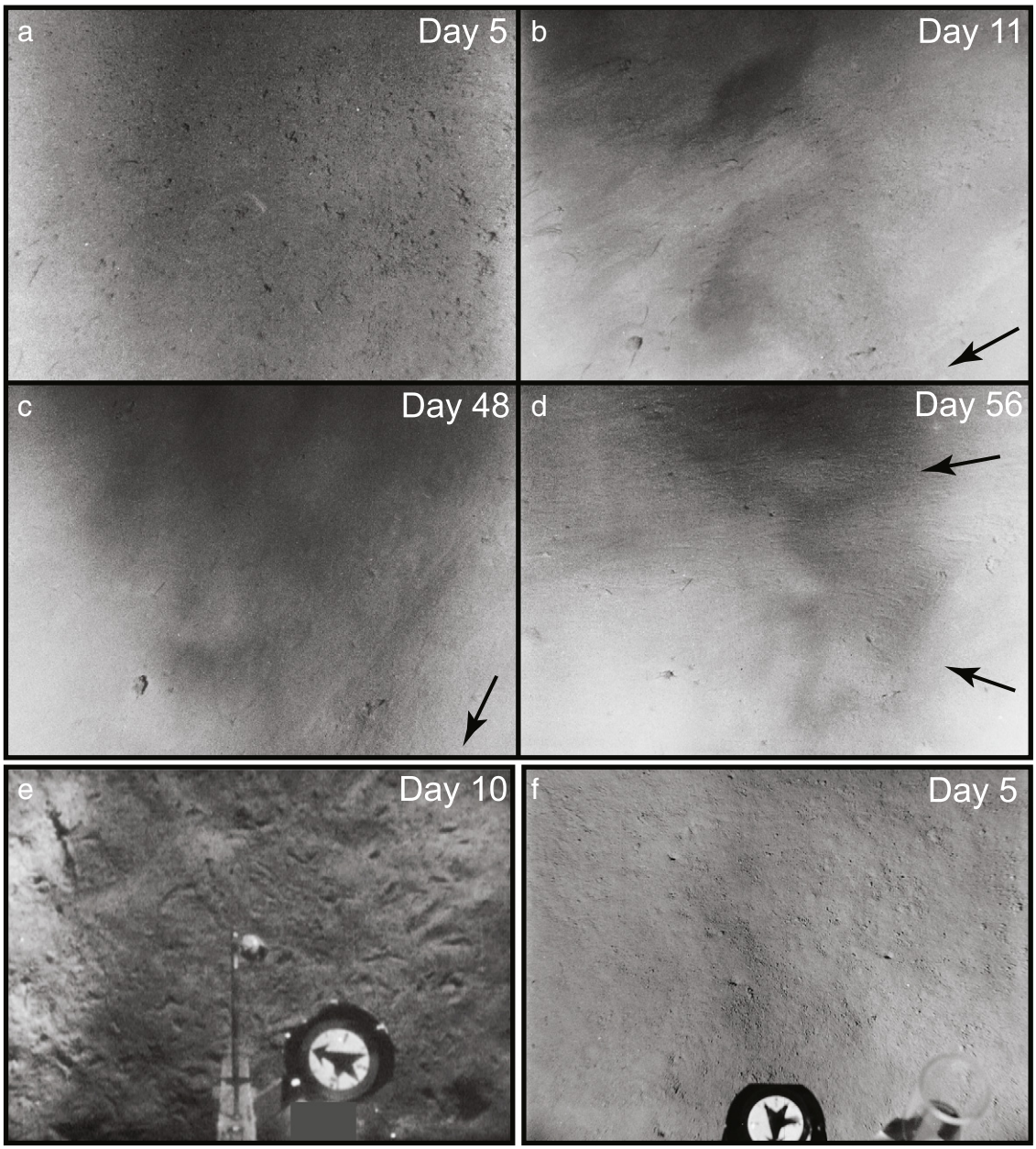

Fig. 12. Bottom photographs taken from time-lapse series at BOM H (a–d), BOM D (e) and BOM T (f). Day of deployment is shown at upper right of photographs and is marked on the E/E_D records in Figs. 2a, b and 3b. Arrows show current direction indicated by seafloor striations and tool marks. Imaged areas are about 125 by 106 cm (a–d), 55 by 41 cm (e), and 61 by 46 cm (f).

smaller PM increase occurred at the end of October at the time that a tropical storm passed about 250 km north of the site.

4.2.5. Mooring E - Eastward Scarp, northeast Bermuda Rise

Mooring E was located on the northeastern Bermuda Rise where a large sedimentary drift is developed well away from the continental margin (Fig. 1) (Laine et al., 1994). The mooring incorporated LTNs at 25 and 313 mab that sampled hourly, together with current meters at 31 and 322 mab. The LTN record at 25 mab and current record at 31 mab are shown here (Fig. 3d, e). Current speeds at 31 mab were generally <10 cm s^{-1}, reaching a maximum of 17 cm s^{-1}.

4.2.6. BOM D - continental slope south of New England

BOM D was set at 1060 m seafloor depth on the continental slope south of Cape Cod for ten months (Fig. 1, Table 1). The deployment was part of the Department of Energy Shelf Edge Exchange Processes (SEEP) study to examine the fate of continental-shelf PM and organic carbon (Biscaye et al., 1994). An LTN at 1.2 mab and a time-lapse camera on the BOM collected data at four-hour intervals. There are no current meter data available for BOM D, but a compass and hanging pendant in the camera's field of view were used to sense the direction and magnitude of currents. Based on pendant deflection, currents were weak to the south (across slope) with little perceptible change in direction or speed during the entire deployment. As shown in Fig. 2a and Table 1, PM concentrations were consistently very low (6–15 μg l^{-1}). Bottom photographs revealed very active benthic epifauna but no current-induced seafloor features (Fig. 12e and Supplemental Video S5).

4.2.7. BOM T - Greater Antilles Outer Ridge

BOM T was deployed at 5133 m depth for 169 days on the north flank of the northwestern Greater Antilles Outer Ridge north of the Puerto Rico Trench (Figs. 1 and 2b, c). The deployment was part of a

study by one of us (BET) to investigate dynamics of sediment transport in AABW at the base of the southern extension of the DWBC. Prior studies there had shown PM concentrations that are relatively low but still significantly elevated relative to areas outside the path of the boundary current (Tucholke, 1975). BOM T had an Aanderaa current meter (with temperature-T, and salinity-S sensors) located 3.5 mab, an LTN (two-hour recording interval, 0.6 mab), and a time-lapse camera with a 4-hour recording interval (Table 1). The site was chosen because earlier bottom photography had shown well-developed sediment ripples and current lineations, and a previous 6-month current meter record indicated a nearly unidirectional, contour-following flow to the southeast at up to 17 cm s^{-1} (Tucholke et al., 1973). Measured currents were only 5–12 cm s^{-1} during the first 66 days of deployment (Fig. 2c) and frequently exhibited a strong semi-diurnal oscillation. The current-meter rotor failed after 66 days. Current direction was consistently in the southeast quadrant throughout the 169-day record, with minor excursions. Data were collected by the LTN (E/E_D of 3.3–6.8, 3–13 μg l^{-1}; Fig. 2b) throughout the deployment. The seafloor was quite uniformly smooth with no current-induced features noted at any time (Fig. 12f).

5. Discussion

We first consider the potential that the mean deep circulation in the western North Atlantic, and the perturbations in that circulation (e.g., EKE and cyclogenesis), have for generating high currents speeds, eroding the seafloor, and thus creating benthic storms. We then discuss how benthic storms observed at fixed BOM and mooring sites appear to relate to deep currents and other impulses that could affect PM concentrations.

5.1. Deep circulation in the western North Atlantic

Hogg (1983) and Hogg et al. (1986) proposed two components of deep circulation in the western North Atlantic basin, each of which has the potential to generate high current speeds. One is a thermohaline circulation that provides a mean flow driven by equatorward spreading of bottom water created at high latitudes (the Atlantic Meridional Overturning Circulation), and the other is an eddy-driven component that forms large-scale mean-recirculation patterns at depths reaching >4000 m in the vicinity of the GS. Recent studies describe the genesis of cyclones and anticyclones beneath GS meanders (Andres et al., 2016) that may provide the eddy-driven component described by Hogg et al. (1986).

5.1.1. Mean bottom-water flow

The thermohaline circulation in the western North Atlantic has both northern and southern high-latitude sources. North Atlantic Deep Water (NADW) consists of Denmark Straight Overflow Water (DSOW) that originates in the Norwegian-Greenland Sea, and Labrador Sea Water (LSW) (Bower et al., 2009, 2011); these form the lower and upper parts, respectively, of the DWBC that flows southward along the western basin margin at depths less than ~4000 m (Luyten, 1977; Andres et al., 2016; Smith et al., 2016). Multiple studies have shown that there is considerable exchange between the DWBC and the interior of the basin (Bower et al., 2009, 2011; Andres et al., 2016; Smith et al., 2016). About half of the DSOW and LSW leaves the DWBC before flowing south of 39°N (Rhein et al., 2015), and that exchange may have increased in the last decade (Andres, 2016). Water below 4000 m is primarily AABW, based on high silicate and low chlorofluorocarbon values. It is sourced from the circum-Antarctic and is confined to the basin south of the Grand Banks (Worthington, 1976; Needell, 1980; Richardson et al., 1981). Both the DWBC and deeper AABW constitute the southward geostrophic flow along the western margin of North Atlantic (see the review by McCave and Tucholke, 1986).

On the Nova Scotian continental rise west of the Grand Banks, Tucholke et al. (1985) studied extensive bottom photographs taken during the HEBBLE program to examine abyssal current activity. Estimated current speeds in the DWBC between 4000 and 3200 m were low and decreased upslope to long-term near-tranquil conditions, in agreement with short-term current measurements of Richardson et al. (1981). Photographs taken below 4000 m showed significant development of current-controlled bedforms, and in AABW at depths > 4800 m they documented strong currents with long-term, contour-parallel orientation to the southwest.

Farther south along the U.S. continental rise, the mean flow of the DWBC and underlying AABW along the U.S. continental slope and rise is southward and contour-parallel (e.g., Heezen et al., 1966; Tucholke et al., 1973; McCave and Tucholke, 1986). However, there is significant variability in both current speed and direction due to interaction with the GS and associated deep cyclogenesis. Lagrangian float measurements (Bower and Hunt, 2000) and models of chemical tracers (Smith et al., 2016) indicate mean equatorward flow speeds of 3–6 cm s^{-1} along the margin. Still farther south along the Bahama Banks, Antilles arc and over the Greater Antilles Outer Ridge, bottom photographs, current measurements, and hydrographic sections show that both the DWBC and underlying AABW have a mean equatorward flow along bathymetric contours but with some excursions lasting from a few days to two months (Tucholke et al., 1973; Fine and Molinari, 1988). Currents measured on the Greater Antilles Outer Ridge over 4–5 month periods peaked at 17 cm s^{-1} but varied by location and averaged <10–15 cm s^{-1} (Tucholke et al., 1973).

In general, spreading of bottom waters from polar regions appears to occur with mean speeds < 10 cm s^{-1} and with seasonal increases of deep-water transport of only 10–20% in September–February (Dickson et al., 2007; Jochumsen et al., 2012). Although these flows are likely to be helpful for dispersing sediment southward along the western basin margin, they are insufficient to create storm conditions of the magnitude we observe unless there is additional energy input. Other perturbations (e.g., deep cyclones and anticyclones, topographic Rossby waves (TRW), seafloor topography) must be present to generate current velocities sufficient to erode seafloor sediment and mix it into the BML.

5.1.2. Cyclogenesis in the deep western North Atlantic

Early models depicted deep-water circulation (>4000 m) in the subtropical interior of the western North Atlantic as a series of gyres that include some southwest flow along contours of the western margin (Worthington, 1976; Wunsch and Grant, 1982; Hogg, 1983). Later models and measurements demonstrated that deep-water cyclogenesis may drive the deep mean circulation (Hogg et al., 1986; Watts et al., 1995, 2001; Savidge and Bane, 1999; Andres et al., 2016). Johns and Watts (1985, 1986) and Hall and Bryden (1985) made current measurements northeast of Cape Hatteras and observed that occasionally the GS extends coherently to the bottom and that downstream flow events in deep water are associated with lateral shifts of the mid-thermocline current structure. Water-column coherence was also observed at several locations beneath the GS by Pillsbury et al. (1982a, 1982b) and Isley et al. (1990), and it is apparent at CMME-6 to the southeast of BOM S (Fig. 8a–d). All of these observations are explained by cyclogenesis beneath meanders of the GS (Watts et al., 1995; Savidge and Bane, 1999; Andres et al., 2016).

Detailed studies in the SYNOP (Synoptic Ocean Prediction) program at a location between BOM S and mooring A (Fig. 1) showed that deep cyclones and anticyclones often spun up beneath tight GS troughs (cold-core meanders) and crests (warm-core meanders), respectively (Watts et al., 1995; Shay et al., 1995; Johns et al., 1995; Savidge and Bane, 1999; Howden, 2000). Animations of these deep eddies (Watts et al., 2001; www.po.gso.uri.edu/dynamics/WBC/) show highly dynamic cyclonic/anticyclonic structure beneath GS meanders and rings. Once formed, it appears that the deep cyclones/anticyclones can move around erratically as they interact with each other, rather than following a path that is strictly linked with the overhead circulation.

During the last decade, hydrographic, current, and trace chlorofluorocarbon measurements have been made along Line W, a transect passing through the SYNOP area from the continental shelf south of New England to Bermuda (Andres, 2016; Smith et al., 2016). A maximum velocity core of the DWBC between 3500 and 4000 m is matched by elevated values of chlorofluorocarbons (Andres et al., 2016). When no GS meanders were present along Line W, deep equatorward flow was restricted to depths < 4000 m, but when meanders were present (35% of the time) equator-ward flow extended down to 5000 m in deep cyclones. Velocity structure of the cyclones was vertically coherent from ~1500 m to the seafloor where they crossed Line W (Andres et al., 2016). During the SYNOP study in this area anticyclones were also observed 21% of the time (Watts et al., 1995, 2001; Savidge and Bane, 1999), but these flows were not as strong or well organized. Andres et al. (2016) showed that cyclones had radii of ~130 km and radii to maximum velocity of ~55 km. The cyclones lasted 6–9 weeks with swirl speeds up to 50 cm s^{-1} at 3500 m and may have reached down to the benthic boundary layer (Savidge and Bane, 1999). Unfortunately, no turbidity measurements were made during these studies.

Cyclonic/anticyclonic flow very likely accounts for extreme variability of bottom currents observed by Richardson et al. (1981) in the HEBBLE area on the Nova Scotian continental rise (Section 4.2.3). Bottom photographs also suggest that smaller-scale bedforms there are constructed and destroyed by strong, variable-direction currents on 3–6 month time scales (Tucholke et al., 1985).

5.2. Surface and deep eddy kinetic energy in the western North Atlantic

The larger the deep EKE, the greater the likelihood of currents intermittently exceeding the critical bed shear stress for erosion. EKE is generated by several factors including GS meanders and rings, deep cyclones and anticyclones, topographic waves, and possibly atmospheric forcing.

The GS forms time-varying meanders, loops, and rings once it departs from the continental shelf east of Cape Hatteras, creating a region of high surface EKE. Weatherly (1984) and Schmitz (1984) observed that where surface EKE was high in the Western North Atlantic, abyssal EKE was also high although lower in intensity, suggesting that surface EKE may be propagated to the seafloor. We can efficiently identify areas of high surface EKE using satellite data by calculating temporal variability in sea-surface height and assuming geostrophy (Daniault and Menard, 1985; Sandwell and Zhang, 1989; Delworth et al., 2012). The maps of Dixon et al. (2011) and Delworth et al. (2012) are particularly useful for comparison with our data (Fig. 13).

Significant advancements have been made in assimilating thousands of current measurements with eddying general circulation models and tides to generate detailed global maps of near-bottom mean kinetic energy (Fig. 2 of Arbic et al., 2010) as well as equally detailed global maps of energy dissipation in the bottom boundary layer (Figs. 5 and 9 of Arbic et al., 2009; Fig. 3 of Wright et al., 2013). There is significant agreement between their maps of mean kinetic energy 50 mab or energy dissipation and the maps of surface EKE (Fig. 14a of Dixon et al., 2011). Their maps show high mean kinetic energy or high energy dissipation rates in the vicinity of the GS that match the highs in our map of excess benthic PM load (Figs. 6 and 13), with the most intense nepheloid layers being at depths deeper than the DWBC. Hollister and McCave (1984) noted a similar correlation between regions of strong nepheloid layers determined by Biscaye and Eittreim (1977) and others (e.g., Kolla et al., 1976; Ewing and Connary, 1970) and areas of high EKE as mapped for surface waters by Wyrtki et al. (1976) and Cheney et al. (1983). These correlations indicate that the variability in currents, deep cyclogenesis, TRWs, and eddy dissipation associated with the GS is more important in eroding seafloor sediments than is the mean flow of the DWBC.

5.3. Perturbations by topographic Rossby waves and mesoscale eddies

Hamilton (2007) described TRWs as low-frequency vorticity waves that generally occur deeper than 1000 m, are significantly influenced by deep stratification, and require a sloping bottom that creates a change in potential vorticity as the wave propagates. TRWs and bottom-trapped TRWs (BTRWs) have been observed to induce energetic deep flows along the continental slope in the western North Atlantic (Thompson, 1971, 1977; Thompson and Luyten, 1976; Hogg, 1981; Louis et al., 1982; Kelley and Weatherly, 1985; Pickart, 1995; Miller et al., 2007). TRWs were also detected in the SYNOP program. Watts et al. (2001) suggested that TRWs either originated somewhere to the east of the SYNOP study area and were instrumental in initiating the pinch-off of rings, or they were radiated by the ring formation process. But with TRWs there was no obvious relationship between the upper flow and the deep high and low pressure centers (anticyclones and cyclones), which propagated quickly westward.

It has been suggested by several authors (Weatherly and Kelley, 1985; Kelley and Weatherly, 1985; Grant et al., 1985; Welsh et al.,

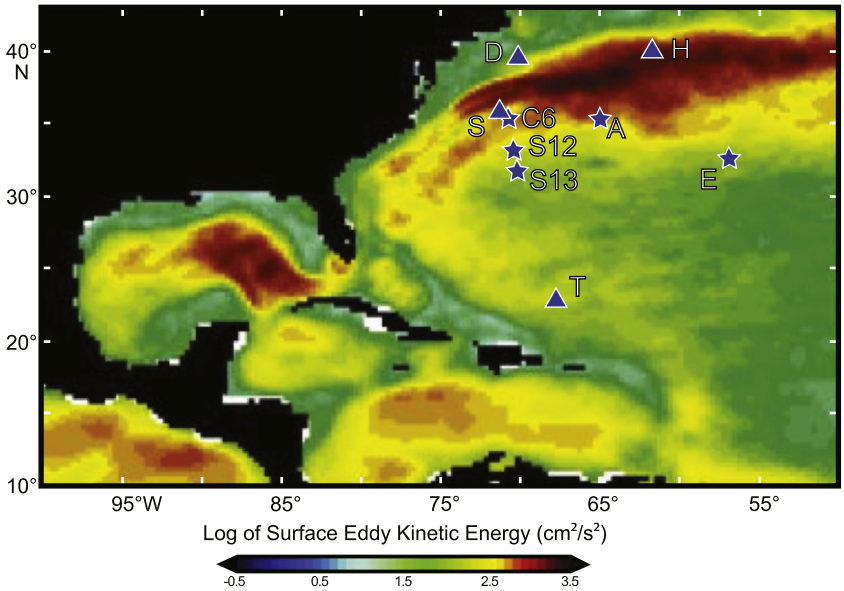

Fig. 13. Map of log of surface EKE based on satellite observations during 2002–2006 (Dixon et al., 2011). BOM and mooring sites are labeled. C6 is current-meter mooring CMME-6.

1991) that surface energy might be propagated through the water column via TRWs that could be generated by meanders and rings of the GS (Hogg, 1981). In the western North Atlantic the source and generation of TRWs between the GS and shelf of the Mid-Atlantic Bight has been attributed to large meanders of the GS and to warm-core rings (Thompson and Luyten, 1976; Hogg, 1981; Pickart, 1995). Analyses by Thompson (1971, 1977) and Thompson and Luyten (1976) show evidence of propagating TRWs below the thermocline with a strong concentration of energy at periods of around 16 days in the North Atlantic. Louis et al. (1982) traced four TRW events to the formation of warm-core rings shed from the GS. Grant et al. (1985) suggested that velocities generated by low-frequency BTRWs, when added to the mean current, could cause turbid benthic events.

5.4. Perturbations by atmospheric forcing

Evidence for correlations between atmospheric storms and deep-sea sediment resuspension has been reported in the studies of Gardner and Sullivan (1981) and Isley et al. (1990). Gardner and Sullivan (1981) recorded a 20-fold increase in PM concentration when the fast-moving hurricane Evelyn passed within 40 km of mooring A in mid-October (Fig. 3c). Of the 14 events of turbid bottom water in the western North Atlantic reported by Isley et al. (1990), over half were initiated within a day of the passage of rapidly propagating (>800 km day^{-1}) atmospheric storms. These correlations suggest that atmospheric forcing can enhance currents and EKE in bottom waters and that the frequent passage of hurricanes and tropical storms through the western North Atlantic may play a role in generating benthic storms and maintaining the BML.

5.5. Observations of benthic storms at BOM and mooring sites

Although records from any one of the three instruments used with the BOM can indicate the likely occurrence of a benthic storm, the combination of current meter, nephelometer, and photographic measurements provides a much more comprehensive assessment of bottom boundary layer conditions than is possible with any of the instruments alone. We have only one deployment (BOM S) where all three instruments functioned and recorded storms. Benthic storms are indicated in LTN records at several other sites, and we consider all of these here in the context of available current or photographic data that document the state of bottom-current activity.

There are caveats that must be considered when interpreting benthic storms from increases in LTN signals. Moored optical sensors provide a PM concentration proxy at a single location and fixed height above the seafloor. Thus it is possible that an increase in current speed, which would thicken the BML (Armi and D'Asaro, 1980) and the nepheloid layer, could be interpreted as a benthic storm, even if the current was not strong enough to erode the local seafloor. In addition to BML thickness variations, transport of turbid water from a distant storm (i.e., as a storm tail) by a meandering current filament or deep eddy could cause an increase in the LTN signal without any local sediment resuspension. In light of such factors, it is necessary to have local information on current intensity, together with vertical PM gradients above the seafloor and/or data on seafloor modification, in order to properly identify a benthic storm as a local event. In the following we consider how these factors may relate to identifying benthic storms at BOM and mooring sites.

5.5.1. BOM S and nearby mooring CMME-6

BOM S and mooring CMME-6 were located in an area of moderately high EKE associated with the GS (Fig. 13). We are not aware of any atmospheric storms that passed within 100 km of these sites during their deployment.

At BOM S, a 40-day period of predominantly cross-slope currents with peak currents of 34 cm s^{-1} in mid-June through July included three periods of elevated PM concentration labeled storms I, II and III (Figs. 5b–e and 9). These storms each lasted 6–8 days based on PM concentration, which exceeded 1000 μg l^{-1}. In each case the PM values began to increase when current speed exceeded ~20 cm s^{-1}, and the PM maxima correlate well with peak current speeds observed in the current record (Fig. 5b, e). Seafloor photographs were clouded during storms I and II although the seafloor was still visible. During storm III the seafloor and compass were totally obscured due to high turbidity.

The transmissometer record at 38 mab on mooring CMME-6 (Table 1) provides strong corroboration of the BOM S data, and most of the time currents at the two locations were visually very coherent (Fig. 8d, e). Peaks in CMME-6 beam attenuation closely match the BOM S current and E/E_D (PM) peaks during storms I–III (Fig. 5e, f), showing that the minimum diameter of the benthic storms was >16 km and vertical mixing was >38 mab (the height of the CMME-6 transmissometer). Unfortunately, there was instrumental drift of beam attenuation in the CMME-6 transmissometer with time, so we cannot quantitatively compare PM concentrations at the two sites.

Before storms I-III, bottom photographs at BOM S showed two ~8-cm-wide depressions in the seafloor with a variety of well-defined animal tracks (Fig. 11, day 1; Supplemental Video S4). As currents shifted to the southeast and PM concentrations increased, sediment cornices began to develop on the north sides of the depressions. Following storms I and II (currents to the southeast at 15–30 cm s^{-1}), the photographs show that some tracks were covered or obliterated and the seafloor was strongly lineated in a NW-SE direction (Fig. 11, day 44). The cornices and much of the surface sediment were then eroded by strong southeasterly, cross-slope currents (up to 30 cm s^{-1}) during storm III, and the seafloor subsequently looked scoured (Fig. 11, compare days 1, 44, and 72). The coincidence of PM peaks, high current speeds, and photographic evidence for seafloor lineations and scouring indicates local erosion of the seafloor during these three benthic storms.

Satellite images of sea surface temperature give a general view of the position of the GS, meanders in the GS, and location of detached cold-core rings during the BOM S deployment (Fig. 5a). GS charts of this vintage unfortunately were hand-drawn and usually published weekly, which precludes tracing meander/ring configurations in detail and on a finer timescale. However, the GS was wandering north and south over BOM S from the time of deployment until mid September (about day 110, Fig. 5a), and both the BOM S and CMME-6 records show that bottom currents were flowing to the southeast during storms I-III (Figs. 8 and 9). At the time of these storms, a meander was seen on July 14, and then a cold-core GS ring moved westward and was located due south of BOM S on July 28 during storm III (Fig. 5a).

During the 5.5-month period following storm III (days 63 to 230, August to mid January), currents shifted to alternating NE and SW flows at speeds that averaged about 10 cm s^{-1}, and PM concentrations were generally low (Figs. 5 and 9). Bottom photographs show that the seafloor became moderately lineated in a SW-NE direction, consistent with the dominantly along-slope currents. The GS moved slightly north of BOM S during early September so that the BOM was under Sargasso Sea water until January. The general pattern of slow flow during this period was interrupted by three current events with peak speeds of 20 cm s^{-1} or more (centered on days 86, 140, and 158). In late August (days 85–90) northeasterly currents reached nearly 30 cm s^{-1} (possibly a direct effect of the GS, which was directly overhead; Figs. 5b and 9) and bottom photographs show that new SW-NE striations appeared in the sediment. However, the PM concentration increased only slightly (doubled from low values, Fig. 5e) compared to the 10-fold increase during storms I–III, even though the current speed was nearly equivalent to that during storms II and III. Thus, currents of the same magnitude, even at the same location, do not necessarily cause the same increase in turbidity. Given the scoured appearance of the seafloor after storm III, we speculate that easily eroded sediment/phytodetritus had been removed from the area during storms I–III, so little increase in PM occurred during this high-speed current event.

Current speeds reached 20 cm s^{-1} twice in October (days 140–142 and 155–160, Fig. 5b) when the GS was north of BOM S, but PM increased slightly only during the second event. In the preceding 1.5 months currents had intermittently reached 15 cm s^{-1}, which may have kept the seafloor clear of easily eroded sediment, thus explaining the lack of an LTN signal during the first event. Subsequently, during days 151–154, bottom photographs showed strong SW-NE striations, and then a large ball of Sargassum was caught on the compass, roughening the underlying sediment. During days 155–160 the photographs showed that the >20 cm s^{-1} current was strong enough to smooth this rough bottom considerably. These observations allow several possibilities for the small PM increase during the second event:

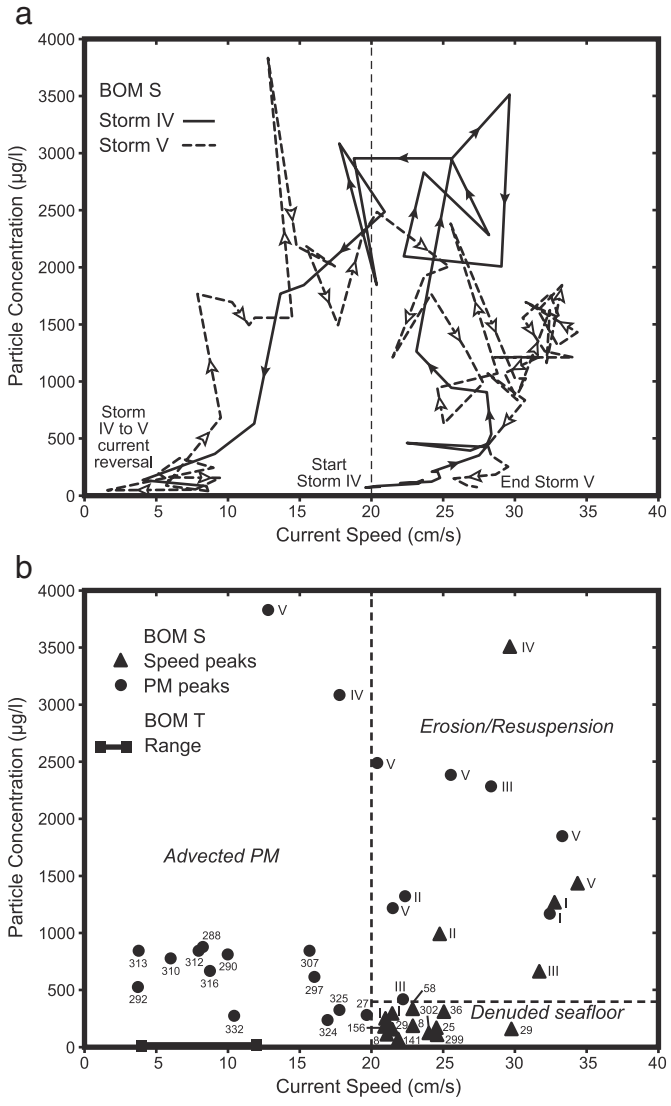

Fig. 14. Plots of current speed versus PM concentration for the two BOM deployments in the western North Atlantic that had current, LTN, and bottom-photograph records. a) Time progression of storms IV and V at BOM S, sampled at 4-h intervals. b) Point values extracted from the complete record of BOM S. Triangles are current-speed peaks > 20 cm s^{-1} with corresponding PM values, and circles are PM peaks > 200 µg l^{-1} with corresponding current speeds. Storm I–V points are labeled and numbers are deployment-day dates (Fig. 5e). Note that the range of values for BOM T (squares) is much lower than for BOM S. Both BOM S and BOM T had near-bottom current meter measurements (6.7 and 3.5 mab respectively) and LTN records (1.2 and 0.6 mab respectively). The plot is validated by time-lapse seafloor photography at BOM S and indicates that current speeds greater than ~20 m s^{-1} are necessary to erode the seafloor (erosion field) but may not be sufficient for erosion if the seafloor has previously been swept clean and stress hardened (denuded seafloor). Seafloor erosion is unlikely at lesser speeds (advected PM field) and high-PM events (>200 µg l^{-1}) in this field most likely represent storm tails. See text for discussion.

1) it may have been related to local erosion by the strong currents, 2) it represented an increase in BML thickness, or 3) it was a storm tail advected from outside the area.

Current speeds in November to mid-January were generally low (~10 cm s^{-1}), and this may have allowed sediment accumulation. Slight fluctuations in PM during this period could be due to minor local resuspension, changes in BML thickness, or advection. Bottom photographs in October–December show some new large animal tracks but no strong current influence.

Two major benthic storms (IV and V) occurred from late January to the beginning of February (Figs. 4a, b and 5), scouring sediment that had accumulated during the previous 2.5 months. The time progression of these storms is shown in a PM vs. current-speed plot in Fig. 14a. During storm IV, the current exceeded 20 cm s^{-1} to the northeast for about 5 days, particle concentrations increased to ~3000 µg l^{-1}, and the seafloor was obscured for two days in bottom photographs. The PM increase associated with this storm began when the current exceeded ~20 cm s^{-1}, and it later tailed off sharply as currents dropped below ~20 cm s^{-1} (Figs. 4a, b and 14a). Between storms IV and V the current slowed to <2 cm s^{-1}, rotated 180° within a few days, and then accelerated to the southwest (Fig. 5b, c and 9). During this reversal, PM concentrations dropped to near-background levels for about one day (likely due to a decrease in erosion, not particle settling) and photos of the seafloor showed strong lineations indicating sediment movement to the northeast (Fig. 11, day 240). The change in current direction between storms IV and V occurred not only near the seafloor, but also through much of the water column, with similar velocities at 2800, 3400, and 4160 m as measured at CMME-6 (Fig. 8). This agrees with the velocity coherence with depth in the vicinity of the GS noted by others (Hogg et al., 1986; Johns and Watts, 1985; Isley et al., 1990; Savidge and Bane, 1999; Andres et al., 2016).

During storm V, current speeds reached up to 34 cm s^{-1} to the southwest and the seafloor was obscured in photographs for six days, with particle concentrations reaching peak values of 2500–3800 µg l^{-1} (Fig. 14a). High PM values in storm V began well before (~3 days) the current reached 20 cm s^{-1}. Considering this and the current reversal (Figs. 5b and 9), it appears likely that the bolus of high-PM water advected to the northeast during storm IV was carried back to the southwest, either comprising or contributing to the high PM of storm V. Currents generally increased as the storm progressed, but at the same time PM values dropped (Figs. 4a, b and 14a). At the end of the storm, currents were still >25 cm s^{-1} but PM decreased sharply to background levels. These observations suggest that erodible sediment was largely removed during the prior storm IV and perhaps during the first part of storm V. Following storm V, reworked surface sediments clearly showed lineations and "crag-and-tail" features indicating sediment transport to the southwest (Fig. 11, day 250) and the two depressions in the viewing area were completely filled with sediment.

Storms IV and V appear to have been associated with formation of a GS ring (Fig. 5a). A cold-core meander developed above the BOM from 5 to 12 January, and by 2 February the meander started detaching as a ring that moved southwest of the BOM, becoming completely detached from the GS by 9 February. Passage of the meander over BOM S was synchronous with the strong NE flow (12–23 January) and SW flow reversal (23 January to 13 February).

The PM peaks of storms IV and V at CMME-6 lag those at BOM S by 2–4 days (Fig. 5e, f). This likely reflects the shifting position of deep currents associated with the GS ring. It should be noted, however, that PM concentrations at BOM S were measured 1.2 mab while at CMME-6 they were measured 38 mab; thus the delay in sensing PM at CMME-6 could reflect the time it took for the BML to thicken and mix resuspended sediment to this height.

Following storm V, from mid-February to the end of April, currents at BOM S reached 20–25 cm s^{-1} three times and PM concentrations intermittently reached 100's of µg l^{-1}, but there was no correlation between current speed and PM (Fig. 5b, e). In time-series photographs

taken throughout this period the seafloor showed small-scale burrows and tracks with minimal indication of current effects (Fig. 11, day 333), although it became increasingly difficult to see seafloor details because the strobe light had weakened. The photographs were frequently clouded during February–April, but the seafloor was still visible. During this part of the deployment the GS ring moved around, seeming to merge with the GS briefly and then again becoming a distinct ring that stayed in the vicinity of both BOM S and the GS.

Peak current events and peak PM events for the complete record of BOM S are summarized in the PM vs. current-speed plot in Fig. 14b. With little exception, data for major benthic storms fall in a field where currents exceeded 20 cm s^{-1}, PM was high, and seafloor erosion was visually documented. One exception is during the later part of storm IV where currents were decreasing but PM remained high (Fig. 14a). This is interpreted to represent continued advection of PM mixed in the BML from 'upstream' as currents subsided. Another exception is the 3800 μg l^{-1} PM peak of storm V where PM increased well before current speed increased (Fig. 4a, b). As already noted, this likely represents a return flow, back over BOM S, of PM eroded and resuspended during storm IV (Fig. 14a, b).

There are numerous events of high current speed (>20 cm s^{-1}) that correlate with low PM (Fig. 14b). These fall in a field where the seafloor appears to have been stress hardened and no significant erosion occurred. This includes the end of storm V when currents were still >20 cm s^{-1}, but PM was decreasing because no easily erodible sediment remained (Fig. 14a). Within the field of high current speed and low PM, minor PM events are interpreted to represent advection of storm tails or thickening of the BML.

A third field in Fig. 14b encompasses events of low current speed (<20 cm s^{-1}), low to moderate PM peaks, and an absence of visual seafloor erosion. Here, all the PM excursions are thought to represent advection of storm tails from distant events. Overall, the BOM S results are consistent with prior observations that current speeds exceeding ~20 cm s^{-1} are required to erode typical seafloor sediments in the western North Atlantic basin, but they also show that such speeds are not sufficient to erode the seafloor if it is stress hardened by preceding events. Conversely, moderate to significant PM events can occur in the presence of weak currents, but these appear consistently to represent storm tails from prior or distal events.

Considering the full record of current speed at BOM S, spectral analysis shows peaks at diurnal and semi-diurnal periods (Fig. 10a, b), but there is no strong peak in the nephelometer data at those periods (Fig. 10c); thus we conclude that PM increases were not dominated by tidal flows. The only E/E_D peaks in the nephelometer spectrum are broad-band peaks at 7.5 and 10 days, and the only peak near these frequencies in the current record was a broad peak around 16 days, which is in the range of TRW periods (10–100 days; Hamilton, 2009). Watts et al. (2001) and Savidge and Bane (1999) showed in the SYNOP study that cyclones develop beneath tight cold-core meander troughs and anticyclones develop beneath warm-core meander crests of the GS. We suggest that the cold-core trough/ring above BOM S during storms IV and V generated a cyclone that caused the benthic storms. This is the first time that a deep-sea benthic storm has been attributed to formation of a GS meander above a mooring site based on simultaneous measurements of near-bottom and water-column currents, EKE, PM, and time-series photographs of the seafloor.

It is not just the presence of the GS, but the meandering motion, that generates rotational flow at depth. Meanders can turn into rings, so rotational flow can exist beneath rings as well, and cyclonic flow can generate anticyclones in surrounding water (Watts et al., 2001). Furthermore, once a deep cyclone is spun up, it might not be fixed beneath a surface meander or ring of the GS; it might move about unpredictably, making it difficult to correlate Gulf Stream surface features with activity at depth. During storms I-III a cold-core ring pushed westward, passing 30 km south of BOM S. Thus, a deep cyclone may account for the strong southeasterly currents during storms I-III (Fig. 5a, e). This could also be the situation in the last two months of the record, where there is no definitive correlation of the complicated GS/ring location with the BOM current and PM record. The lack of correlation could also be an effect, at least partly, of the limited temporal/spatial resolution of the early GS analysis charts. A deep cyclone, or possibly TRWs, during this period could account for PM events occurring as storm tails, independent of current speed.

5.5.2. Moorings S12 and S13

Moorings S12 and S13 were located in areas of moderate to low EKE, respectively, associated with the GS (Fig. 13). No hurricanes or tropical storms are known to have passed near either S12 or S13 during their deployment.

During the 7.5 months that the S12 LTN recorded, there were a number of PM peaks (Figs. 4c and S2) but only one of these, in late October (Fig. S2), directly correlates with current speed > 20 cm s^{-1} (note that LTNs at S12 and S13 were attached 38 mab compared with ~1 mab for BOM LTNs). This event had a peak current of about 25 cm s^{-1} and peak PM of only 200 μg l^{-1}. In the absence of bottom photographic data and/or an additional LTN record closer to the seafloor, we cannot tell if the increased PM represented an advected storm tail, an increase in BML thickness, or local erosion. At the time of this event, a GS ring was about 70 km WNW of S12 (Fig. S2).

PM peaks of 250–300 μg l^{-1} at the end of June (Fig. 4c) and in September (Fig. S2) occurred when currents were <15–18 cm s^{-1}. A stronger, double-peaked PM event in early August initiated about two days after peak current speeds of 35 cm s^{-1} had dropped to ~20 cm s^{-1}, with the second peak occurring before the current again increased. There was a cold core ring 20–50 km to the northwest of S12 during June and in early November 1983, but neither the GS nor rings passed over the site while the LTN recorded. Thus, while some of these current and PM events occurred when GS rings were nearby, others did not, suggesting that it is possible that some of the events represent advection from other locations by variable bottom-currents or eddies.

After the LTN stopped functioning there were times when GS rings and meanders were close to, and on top of S12, but near-bottom current speeds up until July averaged ~10 cm s^{-1} and never reached 20 cm s^{-1} (Fig. S2). The rings and meanders disappeared in later maps at the time that near-bottom current speeds increased in July and August 1984. It is possible that the ring's surface temperature expression was lost due to large-scale surface warming, yet deep cyclones or TRWs remained and generated the increased current speeds.

At S13, PM concentrations started at very high values of ~4000 μg l^{-1} and decreased steadily to ~100 μg l^{-1} during the following week, with only minor increases occurring later (Figs. 4e and S3). Currents were only about 17 cm s^{-1} at time of the initial PM peak and never exceeded 20 cm s^{-1} during the 16-month deployment. The very high PM concentration at the beginning of the record is interpreted to be advection of a storm tail from a distal event because currents were much slower than on other deployments where PM of that magnitude was observed. Subsequent small PM variations show no direct correlation with currents (Fig. 4e, f), and they are interpreted as advection of storm tails across the site. During the LTN recording period, S13 was in an area of relatively low EKE beneath Sargasso Sea water southeast of the GS at all times (Fig. S3). Like S12, later approaches of GS rings and meanders show no clear correlation with increased current speeds, and the highest speeds, during the last three months of the recording period, occurred when the GS was far to the north of the site.

5.5.3. BOM H

BOM H was deployed in an area of high EKE (Figs. 1 and 13) and strong spatial/temporal variation in both GS meander/ring positions and measured bottom currents. We have no atmospheric-storm data from the area of BOM H during the deployment. The 2-month LTN record exhibited four storms (I–IV) characterized by high PM

concentrations (>1000 μg l^{-1}) compared to lower "background" concentrations (80–140 μg l^{-1}) between storms (Fig. 3b).

The two-day current record at the beginning of the deployment showed a maximum speed of 8 cm s^{-1}. The first photograph of the seafloor was July 23 (Fig. 12a, day 5) and it showed tranquil, bioturbated sediment, but between days 7 and 11, LTN values increased rapidly and the seafloor was totally obscured, indicating that currents increased significantly. During storm I, PM reached >4000 μg l^{-1} twice over a period of about 7 days, but it dropped below 200 μg l^{-1} during an intervening ~1-day period, and the photograph on day 11 (Fig. 12b) provided clear evidence that strong currents had reshaped the seafloor. This double peak is reminiscent of the 'lull' between storms IV and V at BOM S and could represent a current reversal wherein PM from the first part of the storm was advected back across the BOM. At the time of storm I, the southwest boundary of a GS meander was over the BOM, and the meander turned into a warm-core ring between 31 July and 7 August at the tail end of the storm (Fig. 3a). The southwest edge of the ring remained over BOM H until the ring was apparently re-entrained in the GS by August 14.

No compass was visible in the photographs so the orientation of the features is unknown. During the ensuing 25-day interval before storm II, the seafloor was quiescent and striations dissipated due to small-scale biological activity creating small pits and mounds. A GS meander crest moved just north of the site after 14 August (Fig. 3a). Although storm I appears to have been associated with the formation of a GS ring above the BOM, the fact that the ring persisted over the site well into the subsequent quiet interval indicates that the surface and deep currents were not directly coupled vertically following the benthic storm. This is consistent with the observation that after spinup, deep cyclones engendered by the GS might move somewhat independently of the surface circulation (Watts et al., 2001; www.po.gso.uri.edu/dynamics/WBC/).

Prior to storm II there were no clear current indicators on the seafloor. Beginning on day 42 the LTN went off scale (>4000 μg l^{-1}) and the seafloor was totally obscured during days 42–47, so we have no photos from that time. When the seafloor again became visible, current striations appeared across the seafloor and were shifted by about 30° from what they had been on day 11 (day 48, Fig. 12c). An increase in turbidity during storm III again obscured the seafloor from day 51 to 55. During this storm the seafloor preserved striations in two different directions; one lineation direction was shifted about 30° from day 48 and the other was shifted by about 80° (day 56, Fig. 12d). Storms II and III occurred during a period when a meander crest of the GS was present around BOM H and closed tighter over the next few weeks (Fig. 3a). This is the condition for maximum current speed in a deep anticyclone (Watts et al., 2001), and movement of an anticyclone could account for the shift in direction of seafloor striations.

Toward the end of storm III there were many small protrusions, bits of debris, and pits, and a large mass of Sargassum (10 × 30 cm) appeared in one photo (day 59). The next day the seafloor was again current swept and the seafloor obscured until the end of storm IV. This settling and rapid removal of debris and multiple striation directions indicate that there was strong variability in current intensity and biologic activity during storm IV. A tight GS meander was over the BOM until the end of the storm on 22 September (Fig. 3a). The next available GS map (23–29 September) showed the GS 80 km south of BOM H and an eddy 100 km to the north, suggesting that the meander had spun off as a warm-core ring.

Beginning between storms III and IV (13 September) and up to the end of the BOM H deployment, a current meter moored 50 mab and 80 km south of BOM H recorded currents up to 73 cm s^{-1} to the southwest (Richardson et al., 1981). The currents were continuously to the southwest and >40 cm s^{-1} from 17 to 22 September, which included the period of storm IV (Fig. 3a). Currents measured at sites 54 km northwest and 115 km southeast of BOM H during the same two-week period flowed northeast at up to 20 cm s^{-1} (Richardson et al., 1981). The bottom-photographic record clearly shows that the storms were associated with elevated current speeds, and both stronger currents and elevated PM were more likely when tight meanders or rings were above or near the site. The GS surface dynamics and extremely high concentrations of PM when meanders and rings were near BOM H are very similar to the dynamics observed at BOM S.

It is apparent from the BOM H record (at a fixed location) that there is strong variability in bottom-current speed and direction that generates benthic storms and abrupt, episodic changes in PM in this region. This variability is also demonstrated in a map of excess PM based on quasi-synoptic nephelometer profiles made across the study area during two separate cruises (Fig. 15). Measurements made over a 12-day period (7–18 July 1979) during R/V Conrad Cruise 22, prior to the deployment of BOM H, show a coherent pattern of high excess PM values in the nepheloid layer focused at stations deeper than ~4800 m, as well as low excess PM in nepheloid layers at shallower seafloor depths (Fig. 15a). R/V Knorr Cruise 74 measurements taken over a 23-day period (9 September–1 October 1979), during which BOM H was recovered, show higher spatial variability in excess PM load, although with the same trend of higher values at greater seafloor depths (Fig. 15b). On September 14 a nephelometer profile and filtered water samples taken five kilometers from BOM H yielded near-bottom particle concentrations of 100–200 μg l^{-1}, in agreement with LTN values from the BOM. The LTN record shows that benthic storms come and go on time scales of days to a week or more and advect PM laterally, which accounts for some of the variability seen in Fig. 15b. The profiles further suggest that high variability in excess PM load can occur at time-averaged spatial scales on the order of 25–50 km.

5.5.4. Mooring A

Mooring A was in an area of typically high EKE (Figs. 1 and 13). The two significant storms at mooring A (Fig. 3c) appear to have been associated with energy transmitted to the seafloor by atmospheric storms. In the first instance, the LTN recorded a nearly 20-fold increase in PM concentration at 20 mab that lagged, by a little more than a day, the nearby passage (40 km) of Hurricane Evelyn in mid-October. The double peak in PM during this storm is similar to but not as well developed as the double-peaked storms at BOM S and BOM H, but it suggests that local recirculation of PM resuspended during the first part of the storm may have occurred. Later, a tropical storm passed within 250 km of the site and it again was followed ~1 day later by a smaller, but significant PM increase. In the absence of current measurements it is unknown whether either of these PM events was due to local seafloor erosion, an increase in BML thickness, or advection from another area.

5.5.5. Mooring E

Mooring E (Laine et al., 1994) was in a region where EKE is generally moderate to low, which is consistent with generally low current speeds measured there (Figs. 1, 3d, e and 13). The LTN record showed mostly small variations in PM concentration, with a background of ~100 μg l^{-1} and PM never reaching >250 μg l^{-1} (Fig. 3d). Current speeds were less than ~10 cm s^{-1} except in mid-August when they reached ~17 cm sec^{-1}, about 2 days after the start of a small PM increase. Laine et al. (1994) noted that the decrease in PM at day 37 followed the decrease in current speed by about 4–5 days, and the PM increase at day 61 followed an increase in current speed after a similar time lag (dotted lines, Fig. 3d, e). These lags could represent thinning of the BML and settling of PM below the LTN at 25 mab as the current waned in the first instance, and BML thickening with upward PM mixing as the current increased in the second instance. The site is well south of the usual path of the GS and no atmospheric storms passed near the site during deployment. This, together with the low current speeds and PM values throughout the record, would also be consistent with the PM events being caused by advection from other areas (Fig. 14b).

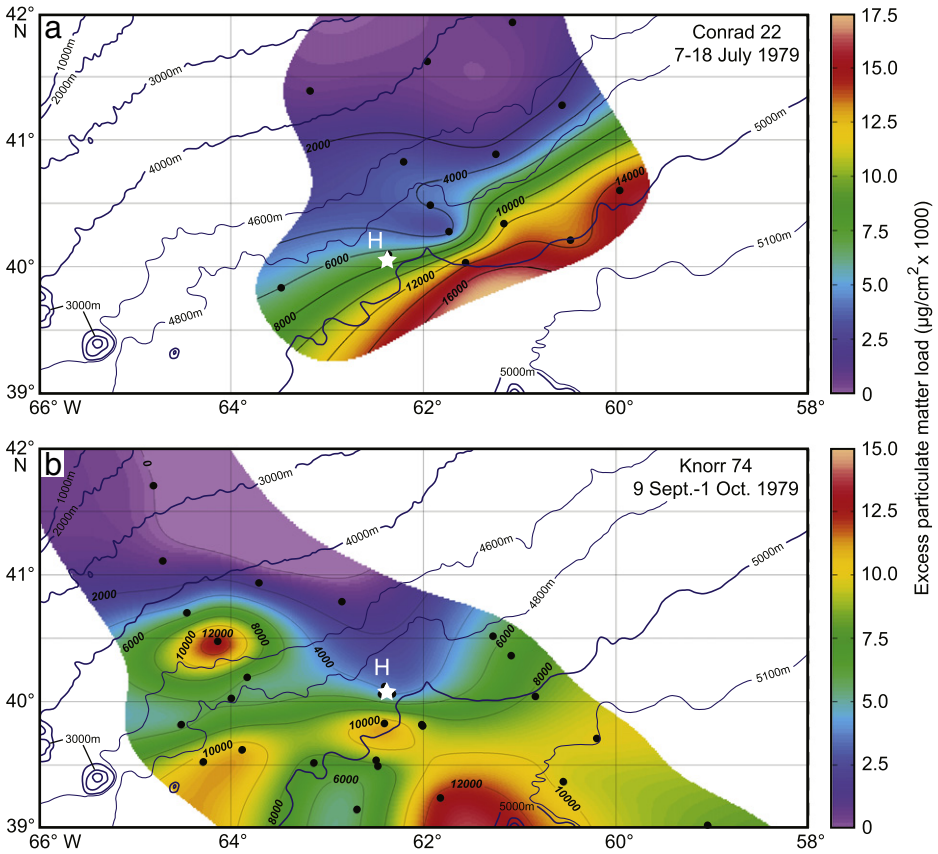

Fig. 15. Maps showing the distribution of excess PM load in the HEBBLE area based on quasi-synoptic vertical nephelometer profiles obtained during two separate cruises. a) Map based on measurements over a 12-day period during Conrad Cruise 22 (7–18 July 1979). b) Map based on measurements over a 23-day period during Knorr Cruise 74 (9 September–1 October 1979). The color scales on the two panels differ slightly. Note the spatial and temporal variability of the excess PM load, but also the consistent, general increase in load with seafloor depth.

5.5.6. BOM D

In contrast to other sites, BOM D (Fig. 2a) was in much shallower water (1060 m), on the upper continental slope (Fig. 1). It was always in slope water north of the GS and its associated meanders/rings, and no severe atmospheric storm activity occurred during the deployment. Based on the dangling pendant in the photos (Fig. 12e), currents were always weak and to the south (across slope) and no current-induced changes in bottom features were noted at any time, which is consistent with the BOM being in an area of low EKE (Fig. 13).

The LTN recorded exceptionally low PM concentrations (6–15 μg l^{-1}) throughout the 308-day recording period. The deployment spanned an entire winter season, but there was no indication from either the LTN record or dangling pendant that cold, dense water cascaded from the adjacent continental shelf. Benthic infauna and epifauna were very active, and numerous changes occurred between most bottom photographs, predominantly in the form of animal tracks that were often added throughout the field of view during the 4 h between frames (see Supplemental Video S5). Photographs showed large crabs making deep footprints, fish swimming by or resting on the bottom, and small worms disturbing the seafloor by burrowing and tunneling. The seafloor constantly changed due to this modification, but LTN E/E_D values 1.2 mab changed very little. The seafloor appeared to be sandy with little fine-grained material, and an absence of fines could explain the lack of significant variation in the LTN signal because currents were not sufficient to resuspend sand. In Fig. 14b, this area would lie in the field of low current, low PM, where benthic storms would not be expected.

5.5.7. BOM T

BOM T was in a very different environment from BOM D, but like BOM D the LTN recorded very low levels of PM (3–13 μg l^{-1}) with little variation (Fig. 2b). At 5133 m on the Greater Antilles Outer Ridge, the site was in AABW, much deeper than the North Atlantic Deep Water that moves south along the western Atlantic margin (Tucholke and Eittreim, 1974). Although previously measured currents were up to 17 cm s^{-1} in this area (Tucholke et al., 1973), BOM T current speeds, which were recorded only during the first one-third of the deployment, were slow (<12 cm s^{-1}, Fig. 2c) and toward the southeast parallel to bathymetric contours. This site was located well south of any influence of the GS and in an area of low EKE, and no severe atmospheric storms passed overhead during the recording period.

No bedform formation or erosion of surface sediments was observed in time-series photographs (Fig. 12f). Several worm burrows < 1 cm in diameter were present and remained unchanged. Tiny pits a few mm in size dotted the seafloor. On four occasions, a brittle star or crab moved through the field of view. Neither current nor faunal effects caused resuspension of fines to create PM excursions in the LTN record.

Considering the BOM T current and LTN records, the site position with respect to the long-term excess PM load (Fig. 1), and its location outside the area of high EKE, this area is primarily depositional, receiving sediments transported southward from high-EKE areas along the eastern North American margin by the mean flow of the DWBC and deeper AABW. Thus it falls predominantly within the advection field of Fig. 14b. Assuming that this regime has persisted over geologic time scales, it is consistent with long-term construction of the Greater Antilles Outer Ridge, with little or no significant seafloor erosion there.

6. Conclusions

We reviewed known characteristics and proposed origins of the permanent benthic nepheloid layer, and we then investigated how benthic storms relate to this layer in the western North Atlantic Ocean. We

examined the benthic storms using data from two decades of nephelometer profiles, and data from months- to year-long moorings that were variably instrumented with time-lapse nephelometers, current meters, and time-lapse cameras. From our analysis we reach the following conclusions:

1) The mean equatorward geostrophic flow of abyssal currents (the DWBC and underlying AABW) is <10 cm s^{-1}, which is insufficient to erode typical seafloor sediments in the western North Atlantic. Other, more energetic mechanisms are necessary to create benthic storms.
2) The primary source of particulate matter (PM) in the benthic nepheloid layer is seafloor sediment eroded by bottom currents when the critical bed shear stress is exceeded, creating 'benthic storms'. Time-series bottom photographs and nephelometer records, coupled with current-meter measurements, indicate that current speeds exceeding ~20 cm s^{-1} near the seafloor are needed to erode the typically fine-grained sediments in the western North Atlantic basin (Fig. 14b). By comparison, PM sourced from continental shelves, tidal and internal-wave pumping in submarine canyons, and turbidity currents is rarely significant in generating high-PM events that would act to maintain persistent benthic nepheloid layers away from the margins.
3) Time-series nephelometer light-scattering measurements made ~1 m to 38 m above the seafloor on bottom tripods and moorings, respectively, recorded high PM events characterized by light scattering equivalent to concentrations of 300–4000 μg l^{-1} that lasted up to 6–8 days; these events contrast strongly with background levels generally <200 μg l^{-1}. Some of the events can be documented as local benthic storms, i.e. they have measured currents that are consistently or intermittently strong enough to erode seafloor sediment (20–35 cm s^{-1}) coincident with seafloor erosion visible in time-lapse photography (Fig. 14b). Other high PM events occurred in the presence of weak currents where PM was advected from benthic storms in other areas where the seafloor was eroded, i.e. these were storm tails. There were also times when strong currents (>20 cm s^{-1}) with erosive potential were recorded, but they increased PM concentrations by only a factor of 3 or less compared with factors of 10–100 during benthic storms. These events appear to represent situations where most loose detritus and unconsolidated silt and clay had already been removed and the seafloor was 'stress hardened'; further erosion could be produced only by exceptionally strong currents or after bioturbation or settling of new material. Some small PM increases that were produced during strong flows might have been created largely by thickening of the bottom mixed layer (up to or above the instrument height) due to the increased current speed. Observed events of elevated PM in time-series records (both benthic storms and storm tails) generally occur at irregular intervals of weeks to months or more.
4) High PM concentrations in the persistent benthic nepheloid layer, as well as occurrences of benthic storms, often closely match the position of Gulf Stream meanders and rings, as well as the mean intensity of EKE in surface waters as determined from satellite measurements. High surface energy associated with Gulf Stream meanders and rings is propagated downward, sometimes to the seafloor, in the form of cyclones, anticyclones, or topographic waves, generating current speeds sufficient to erode seafloor sediments and create benthic storms. Some time-series records suggest that surface energy added by fast-moving hurricanes or tropical storms can also propagate to the seafloor and generate benthic storm events.
5) The deep eddies engendered by the Gulf Stream (and possibly by atmospheric storms) augment or reduce the mean southerly flow of the DWBC and underlying AABW along the western Atlantic margin in erratic ways. Lagrangian measurements using deep floats or gliders whose location is determined using moored acoustic transponders, together with data telemetry to surface buoys for real time monitoring and directing, are needed to track these currents and relate them to shallower circulation patterns.
6) In addition to being the primary source of PM in the benthic nepheloid layer, benthic storms are also necessary for its maintenance. Outside the region of high EKE and active benthic storms (Fig. 6), PM that is carried equatorward in the benthic nepheloid layer by the DWBC and AABW is not significantly replenished in low-EKE regions, and the layer becomes diluted as PM settles out of the flow. Background levels of PM in the benthic nepheloid layer outside the region of high EKE average <20 μg l^{-1} (and can be <10 μg l^{-1} in mid-basin areas) compared with 20–150 μg l^{-1} in the more energetic environment.
7) Finally, we note that PM scavenges adsorption-prone radionuclides that are used as paleo-productivity proxies and for investigation of modern and paleo-ocean circulation. Our improved understanding of how and where PM in the benthic nepheloid layer is sourced, transported, and deposited will help to determine where such scavenging is most likely to occur and to assess its impact on global biogeochemistry.

Supplementary data to this article can be found online at http://dx.doi.org/10.1016/j.margeo.2016.12.012.

Funding

Funding for construction of the Bottom Ocean Monitor was provided by Lamont-Doherty Geological Observatory (now Lamont-Doherty Earth Observatory). BOM and mooring deployments and data analysis were funded by the Office of Naval Research (contracts N00014-75-C-0210 and N00014-80-C-0098 to Biscaye and Gardner at Lamont-Doherty; Contracts N00014-79-C-0071 and N00014-82-C-0019 at Woods Hole Oceanographic Institution and ONR Contracts N00014-75-C-0210 and N00014-80-C-0098 at Lamont-Doherty Geological Observatory to Tucholke), Sandia National Laboratories (contract SL-16-5279 to Gardner), the National Science Foundation (contract OCE 1536565 to Gardner and Richardson), Earl F. Cook Professorship (Gardner), and the Department of Energy (contract DE-FG02-87ER-60555 to Biscaye).

Acknowledgements

We thank Lawrence Sullivan and his team for their invaluable expertise in preparing and deploying instruments, and collecting and producing quality data from the multiple projects involved in this work over many years and numerous expeditions. We also extend thanks to Mary Parsons, Adele Hanley, Patty Catanzaro, plus personnel aboard numerous ships, and many colleagues for help in collecting these data. Reviews by Pere Puig and an anonymous reviewer were greatly appreciated and helped improve the manuscript.

References

Amos, A.F., Gerard, R.D., 1979. Anomalous bottom water south of the Grand Banks suggests turbidity current activity. Science 203, 894–897.
Anderson, R.F., Mawji, E., Cutter, G.A., Measures, C.I., Jeandel, C., 2014. GEOTRACES: changing the way we explore ocean chemistry. Oceanography 27:50–61. http://dx.doi.org/10.5670/oceanog.2014.07.
Andres, M., 2016. On the recent destabilization of the Gulf Stream path downstream of Cape Hatteras. Geophys. Res. Lett. 43:9836–9842. http://dx.doi.org/10.1002/2016GL069966.
Andres, M., Toole, J.M., Torres, D.J., Smethie Jr., W.M., Joyce, T.M., Curry, R.G., 2016. Stirring by deep cyclones and the evolution of Denmark Strait overflow water observed at line W. Deep-Sea Res. I Oceanogr. Res. Pap. 109, 10–26.
Arbic, B.K., Shriver, J.F., Hogan, P.J., Hurlburt, H.E., McClean, J.L., Metzger, E.J., Scott, R.B., Sen, A., Smedstad, O.M., Wallcraft, A.J., 2009. Estimates of bottom flows and bottom boundary layer dissipation of the oceanic general circulation from global high-resolution models. J. Geophys. Res. 114, C02024. http://dx.doi.org/10.1029/2008JC005072.
Arbic, B.K., Wallcraft, A.J., Metzger, E.J., 2010. Concurrent simulation of the eddying general circulation and tides in a global ocean model. Ocean Model. 32, 175–187.
Armi, L., 1978. Mixing in the deep ocean - the importance of boundaries. Oceanus 21, 14–19.

Armi, L., D'Asaro, E., 1980. Flow structures of the benthic ocean. Journal of Geophysical Research Oceans 85:469–484. http://dx.doi.org/10.1029/JC085iC01p00469.

Armi, L., Millard Jr., R.C., 1976. The bottom boundary layer of the deep ocean. J. Geophys. Res. 81:4983–4990. http://dx.doi.org/10.1029/JC081i027p04983.

Beaulieu, S.E., 2003. Resuspension of phytodetritus from the sea floor: a laboratory flume study. Limnol. Oceanogr. 48, 1235–1244.

Bell, T.H., 1974. Vertical mixing in the deep ocean. Nature 251, 43–44.

Biscaye, P.E., Eittreim, S.L., 1977. Suspended particulate loads and transports in the nepheloid layer of the abyssal Atlantic Ocean. Mar. Geol. 23, 155–172.

Biscaye, P.E., Flagg, C.N., Falkowski, P.G., 1994. The Shelf Edge Exchange Processes experiment, SEEP-II: an introduction to hypotheses, results and conclusions. Deep-Sea Res. II 41, 231–252.

Bishop, J.K.B., Biscaye, P.E., 1982. Chemical characterization of individual particles from the nepheloid layer in the Atlantic ocean. Earth Planet. Sci. Lett. 58, 265–275.

Boss, E., Guidi, L., Richardson, M.J., Stemmann, L., Gardner, W., Bishop, J.K.B., Anderson, R.F., Sherrell, R.M., 2014. Optical techniques for remote and in-situ characterization of particles pertinent to GEOTRACES. Prog. Oceanogr. http://dx.doi.org/10.1016/j.pocean.2014.09.007.

Bower, A.S., Hunt, H.D., 2000. Lagrangian observations of the deep western boundary current in the North Atlantic Ocean. Part I: large-scale pathways and spreading rates. J. Phys. Oceanogr. 30, 764–783.

Bower, A.S., Lozier, M.S., Gary, S.F., Böning, C.W., 2009. Interior pathways of the North Atlantic meridional overturning circulation. Nature 459:243–248. http://dx.doi.org/10.1038/nature07979.

Bower, A.S., Lozier, S., Gary, S.F., 2011. Export of Labrador Sea Water from the subpolar North Atlantic: a Lagrangian perspective. Deep-Sea Res. II 58:1798–1818. http://dx.doi.org/10.1016/j.dsr2.2010.10.060.

Brewer, P.G., Spencer, D.W., Biscaye, P.E., Hanley, A., Sachs, P.S., Smith, C.L., Kadar, S., Fredericks, J., 1976. The distribution of particulate matter in the Atlantic Ocean. Earth Planet. Sci. Lett. 32, 393–402.

Cacchione, D.A., Wunsch, C., 1974. Experimental study of internal waves over a slope. J. Fluid Mech. 66, 223–239.

Cacchione, D.A., Pratson, L.F., Ogston, A.S., 2002. The shaping of continental slopes by internal tides. Science 296, 724–727.

Canals, M., Puig, P., de Madron, X.D., Heussner, S., Palanques, A., Fabres, J., 2006. Flushing submarine canyons. Nature 444:354–357. http://dx.doi.org/10.1038/nature05271.

Cheney, R.E., Marsh, J.G., Beckley, B.D., 1983. Global mesoscale variability from collinear tracks of SEASAT altimeter data. J. Geophys. Res. 88, 4343–4354.

Daniault, N., Menard, Y., 1985. Eddy kinetic energy distribution in the southern ocean from altimetry and FGGE drifting buoys. J. Geophys. Res. 90, 11,877–811,889.

Delworth, T.L., Rosati, A., Anderson, W., Adcroft, A.J., Balaji, V., Benson, R., Dixon, K.W., Griffies, S.M., Lee, H.-C., Pacanowski, R.C., Vecchi, G.A., Wittenberg, A.T., Zeng, F., Zhang, R., 2012. Simulated climate and climate change in the GFDL CM2.5 high-resolution coupled climate model. J. Clim. 25:2755–2781. http://dx.doi.org/10.1175/JCLI-D-11-00316.1.

Dickson, R.R., Rudels, B., Dye, S., Karcher, M., Meincke, J., Yashayaev, I., 2007. Current estimates of freshwater flux through Arctic and subarctic seas. Prog. Oceanogr. 73, 210–230.

Dixon, K.W., Delworth, T.L., Rosati, A.J., Anderson, W., Adcroft, A., Balaji, V., Benson, R., Griffies, S.M., Lee, H.-C., Pacanowski, R.C., Vecchi, G.A., Wittenberg, A.T., Zeng, F., Zhang, R., 2011. Ocean circulation features of the GFDL CM2.6 & CM2.5 high-resolution global coupled climate models. WCRP Open Science Conference, October 2011, Denver, Colorado.

Driscoll, M.L., Tucholke, B.E., McCave, I.N., 1985. Seafloor zonation in sediment texture on the Nova Scotian lower continental rise. Mar. Geol. 66, 25–41.

Eittreim, S., Ewing, M., 1972. Suspended particulate matter in the deep waters of the North American Basin. In: Gordon, A.L. (Ed.), Studies in Physical Oceanography. Gordon and Breach, London, pp. 123–167.

Eittreim, S., Thorndike, E.M., Sullivan, L., 1976. Turbidity distribution in the Atlantic Ocean. Deep-Sea Res. 23, 1115–1127.

Ewing, M., Connary, S., 1970. Nepheloid layer in the North Pacific. Geological Society of America Memoir 126, 41–82.

Ewing, M., Thorndike, E.M., 1965. Suspended matter in deep ocean water. Science 147, 1291–1294.

Fine, R.A., Molinari, R.L., 1988. A continuous deep western boundary current between Abaco (26.5°N) and Barbados (13°N). Deep-Sea Res. 35, 1441–1450.

Gardner, W.D., 1986. Results of the Bottom Ocean Monitor (BOM) at LLWODP Area E-N2 and nephelometers on moorings in the Northwest Atlantic. Sandia Low-Level Waste Ocean Disposal Program Final Technical Report, pp. 1–18.

Gardner, W.D., 1989a. Baltimore Canyon as a modern conduit of sediment to the deep sea. Deep-Sea Res. 36, 323–358.

Gardner, W.D., 1989b. Periodic resuspension in Baltimore Canyon by focusing of internal waves. J. Geophys. Res. 94, 18185–18194.

Gardner, W.D., Richardson, M.J., 1992. Particle export and resuspension fluxes in the western North Atlantic. In: Rowe, G.T., Pariente, V. (Eds.), Deep-sea Food Chains and the Global Carbon CycleNATO ASI Series. Kluwer Academic Publishers, Netherlands, pp. 339–364.

Gardner, W.D., Sullivan, L.G., 1981. Benthic storms: temporal variability in a deep ocean nepheloid layer. Science 213, 329–331.

Gardner, W.D., Richardson, M.J., Hinga, K.R., Biscaye, P.E., 1983. Resuspension measured with sediment traps in a high-energy environment. Earth Planet. Sci. Lett. 66, 262–278.

Gardner, W.D., Biscaye, P.E., Zaneveld, J.R.V., Richardson, M.J., 1985a. Calibration and comparison of the LDGO nephelometer and the OSU transmissometer on the Nova Scotian Rise. Mar. Geol. 66, 323–344 (1985a).

Gardner, W.D., Southard, J.B., Hollister, C.D., 1985b. Sedimentation and resuspension in the western North Atlantic. Mar. Geol. 65, 199–242.

Gardner, W.D., Biscaye, P.E., Tucholke, B.E., 1986. Nepheloid layers, eddy kinetic energy and benthic storms. American Geophysical Union]–>EOS Trans. Am. Geophys. Union 67, 1018.

Grant, W.D., Williams III, A.J., Gross, T.F.A., 1985. Description of the bottom boundary layer at the HEBBLE site: low frequency forcing, bottom stress and temperature structure. Mar. Geol. 66, 219–241.

Hall, M.M., Bryden, H.L., 1985. Profiling the Gulf Stream with a current meter mooring. Geophys. Res. Lett. 12, 203–206.

Hamilton, P., 2007. Deep-current variability near the Sigsbee Escarpment in the Gulf of Mexico. J. Phys. Oceanogr. 37, 708–726.

Hamilton, P., 2009. Topographic Rossby waves in the Gulf of Mexico. Prog. Oceanogr. 82, 1–31.

Hayes, C.T., Anderson, R.F., Fleisher, M.Q., Huang, K.-F., Robinson, L.F., Lu, Y., Cheng, H., Edwards, R.L., Moran, S.B., 2014. ^{230}Th and ^{231}Pa on GEOTRACES GA03, the U.S. GEOTRACES North Atlantic transect, and implications for modern and paleoceanographic chemical fluxes. Deep-Sea Res. II http://dx.doi.org/10.1016/j.dsr2.2014.07.007.

Heezen, B.C., Hollister, C.D., 1972. The Face of the Deep. Oxford Univ. Press, New York (659 pp).

Heezen, B.C., Hollister, C.D., Ruddiman, W.F., 1966. Shaping of the continental rise by deep geostrophic contour currents. Science 152, 502–508.

Hogg, N.G., 1981. Topographic waves along 70° W on the continental rise. J. Mar. Res. 39, 627–649.

Hogg, N.G., 1983. A note on the deep circulation of the western North Atlantic: its nature and causes. Deep-Sea Research Part A. Oceanographic Research Papers 30, 945–961.

Hogg, N.G., Pickart, R.S., Hendry, R.M., Smethie Jr., W.J., 1986. The northern recirculation gyre of the Gulf Stream. Deep-Sea Res. 33, 1139–1165.

Hollister, C.D., Heezen, B.C., 1972. Geologic effects of ocean bottom currents: western North Atlantic. In: Gordon, A.L. (Ed.), Studies in Physical Oceanography - A Tribute to George Wüst on His 80th Birthday, 2. Gordon and Breach, New York, N.Y., pp. 37–66.

Hollister, C.D., McCave, I.N., 1984. Sedimentation under deep-sea storms. Nature 309, 220–222.

Hollister, C.D., Nowell, A.R.M., 1991. HEBBLE epilogue. Mar. Geol. 99, 445–460.

Hotchkiss, F.S., Wunsch, C., 1982. Internal waves in Hudson Canyon with possible geological implications. Deep-Sea Res. 29, 415–442.

Houpert, L., Durrieu de Madron, X., Testor, P., Bosse, A., D'Ortenzio, F., Bouin, M.N., Dausse, D., Le Goff, H., Kunesch, S., Labaste, M., Coppola, L., Mortier, L., Raimbault, P., 2016. Observations of open-ocean deep convection in the northwestern Mediterranean Sea: seasonal and interannual variability of mixing and deep water masses for the 2007–2013 period. Journal of Geophysical Research, Oceans 121. http://dx.doi.org/10.1002/2016JC011857.

Howden, S.D., 2000. The three-dimensional secondary circulation in developing Gulf Stream meanders. J. Phys. Oceanogr. 30, 888–915.

Isley, A.E., Pillsbury, R.D., Laine, E.P., 1990. The genesis and character of benthic turbid events, northern Hatteras Abyssal Plain. Deep-Sea Res. 37, 1099–1119.

Jerlov, N.C., 1953. Particle distribution in the ocean. Reports of the Swedish Deep-Sea Expedition 3, pp. 73–97.

Jochumsen, K., Quadfasel, D., Valdimarsson, H., Jónsson, S., 2012. Variability of the Denmark Strait overflow: moored time series from 1996–2011. J. Geophys. Res. 117 (C12003):2012. http://dx.doi.org/10.1029/2012JC008244.

Johns, W.E., Watts, D.R., 1985. Gulf Stream meanders: observations on the deep currents. J. Geophys. Res. 90, 4819–4832.

Johns, W.E., Watts, D.R., 1986. Time scales and structure of topographic Rossby waves and meanders in the deep Gulf Stream. J. Mar. Res. 44, 267–290.

Johns, W.E., Shay, T.J., Bane, J.M., Watts, D.R., 1995. Gulf Stream structure, transport, and recirculation near 68°W. J. Geophys. Res. 100, 817–838.

Johnson, D.A., Lonsdale, P.F., 1976. Erosion and sedimentation around Mytilus Seamount, New England continental rise. Deep-Sea Res. 23, 429–440.

Johnson, D.A., McDowell, S.E., Sullivan, L.G., Biscaye, P.E., 1976. Abyssal hydrography, nephelometry, currents and benthic boundary layer structure in the Vema Channel. J. Geophys. Res. 81, 5771–5786.

Kao, S.J., Dai, M., Selvaraj, K., Zhai, W., Cai, P., Chen, S.N., Yang, J.Y.T., Liu, J.T., Liu, C.C., Syvitski, J.P.M., 2010. Cyclone-driven deep sea injection of freshwater and heat by hyperpycnal flow in the subtropics. Geophys. Res. Lett. L21702. http://dx.doi.org/10.1029/2010GL044893.

Kelley, E.A., Weatherly, G.L., 1985. Abyssal eddies near the Gulf Stream. J. Geophys. Res. 90, 3151–3159.

Klein, H., Mittelstaedt, E., 1992. Currents and dispersion in the abyssal Northeast Atlantic: results from the NOAMP field program. Deep-Sea Res. 39, 1727–1745.

Kolla, V., Sullivan, L., Streeter, S.S., Langseth, M.G., 1976. Spreading of Antarctic bottom water and its effects on the floor of the Indian Ocean inferred from bottom water potential temperature turbidity, and sea-floor photography. Mar. Geol. 21, 71–189.

Krone, R.B., 1993. Sedimentation revisited. In: Mehta, A.J. (Ed.), Nearshore and Estuarine Cohesive Sediment Transport. American Geophysical Union, Washington, D. C., pp. 108–125.

Laine, E.P., 1977. Geological Effects of the Gulf Stream System in the North American Basin. (Ph.D. Dissertation). Massachusetts Institute of Technology – Woods Hole Oceanographic Institution Joint Program in Oceanography.

Laine, E.P., Hollister, C.D., 1981. Geological effects of the Gulf Stream system on the northern Bermuda Rise. Mar. Geol. 39, 277–310.

Laine, E.P., Gardner, W.D., Richardson, M.J., Kominz, M., 1994. Abyssal currents and advection of resuspended sediment along the northeastern Bermuda Rise. Mar. Geol. 119, 159–171.

Lampitt, R.S., 1985. Evidence for the seasonal deposition of detritus to the deep-sea floor and its subsequent resuspension. Deep-Sea Res. 32, 885–897.

Louis, J., Petrie, B., Smith, P., 1982. Observations of topographic Rossby waves on the continental margin off Nova Scotia. J. Phys. Oceanogr. 12, 47–55.
Luyten, J.R., 1977. Scales of motion in the deep Gulf Stream and across the continental rise. J. Mar. Res. 35, 49–74.
McCave, I.N., 1984. Size spectra and aggregation of suspended particles in the deep ocean. Deep-Sea Res. 31, 329–352.
McCave, I.N., 1985. Properties of suspended sediment over the HEBBLE area on the Nova Scotian rise. Mar. Geol. 66, 169–188.
McCave, I.N., 1986. Local and global aspects of the bottom nepheloid layers in the world ocean. Netherlands Journal of Sea Research]–>Neth. J. Sea Res. 20, 167–181.
McCave, I.N., Hall, I.R., 2006. Size sorting in marine muds: processes, pitfalls, and prospects for paleoflow-speed proxies. Geochem. Geophys. Geosyst. 7:Q10N05. http://dx.doi.org/10.1029/2006GC001284.
McCave, I.N., Tucholke, B.E., 1986. Deep current-controlled sedimentation in the western North Atlantic. In: Vogt, P.R., Tucholke, B.E. (Eds.), The Geology of North AmericaThe Western North Atlantic Region vol. M. Geological Society of America, Boulder, CO, pp. 451–468.
Miller, A.J., Neilson, D.J., Luther, D.S., Hendershott, M.C., Cornuelle, B.D., Worcester, P.F., Dzieciuch, M.A., Dushaw, B.D., Howe, B.M., Levin, J.C., Arango, H.G., Haidvogel, D.B., 2007. Barotropic Rossby wave radiation from a model Gulf Stream. Geophys. Res. Lett. 34, L23613. http://dx.doi.org/10.1029/2007GL031937.
Needell, G.J., 1980. The distribution of dissolved silica in the deep western North Atlantic Ocean. Deep-Sea Research Part A. Oceanographic Research Papers 27, 941–950.
Pak, H., 1983. Fluctuations of beam-attenuation coefficient in the lowest 2 m on the continental rise off Nova Scotia. Mar. Geol. 51, 77–97.
Pak, H., Zaneveld, J.R.V., 1983. Temporal variations of beam attenuation coefficient on the continental rise off Nova Scotia. J. Geophys. Res. 88, 4427–4432.
Palanques, A., Puig, P., Mikel, L., Renate, S., 2009. Deep sediment transport induced by storms and dense shelf-water cascading in the northwestern Mediterranean basin. Deep-Sea Res. I 56, 425–434.
Partheniades, E., 1965. Erosion and deposition of cohesive soils. J. Hydraul. Div. ASCE 91, 105–139.
Pickart, R.S., 1995. Gulf Stream-generated topographic Rossby waves. J. Phys. Oceanogr. 25, 574–586.
Pillsbury, R.D., Bottero, J., Pittock, G., Root, D.C., Simpkins III, J., Laine, E.P., 1982a. Data Report for Current Meters on Moorings CMME-2, 1981–82; Atlantic Study Areas E-N3. Oregon State University, School of Oceanography, Corvallis. Report OSU-16.
Pillsbury, R.D., Bottero, J., Still, R.E., Laine, E.P., 1982b. Data Report for Current Meters on Moorings CMME-1, 1980–82; Atlantic Study Areas E-N3. Oregon State University, School of Oceanography, Corvallis. Report OSU-15.
Pillsbury, R.D., Bottero, J., Pittock, G., Root, D.C., Simpkins III, J., Laine, E.P., 1984. Data Report for Current Meters on Moorings CMME-4, 5, 6, and BOM, 1982–83; Atlantic Study Areas E-N2 and E-N3. Oregon State University, School of Oceanography, Corvallis. Report OSU-22.
Pillsbury, R.D., Barstow, D., Bottero, J., Moore, B., Pittock, G., Root, D.C., Simpkins III, J., Laine, E.P., 1985. Data Report for Current Meters on Moorings CMME-9, 11, 12, and 13, 1983–84; Atlantic Study Areas E-N2 and E-N3. Oregon State University, School of Oceanography, Corvallis. Report OSU-25.
Puig, P., Durrieu de Madron, X., Salat, J., Schroeder, K., Martín, J., Karageorgis, A.P., Palanques, A., Roullier, F., Lopez-Jurado, J.L., Emelianov, M., Moutin, T., Houpert, L., 2013a. Thick bottom nepheloid layers in the western Mediterranean generated by deep dense shelf water cascading. Prog. Oceanogr. 111, 1–23.
Puig, P., Greenan, B.J.W., Li, M.Z., Prescott, R.H., Piper, D.J.W., 2013b. Sediment transport processes at the head of Halibut Canyon, eastern Canada margin: an interplay between internal tides and dense shelf-water cascading. Mar. Geol. 341, 14–28.
Puig, P., Palanques, A., Martin, J., 2014. Contemporary sediment-transport processes in submarine canyons. Annu. Rev. Mar. Sci. 6, 53–77.
Rhein, M., Kieke, D., Steinfeldt, R., 2015. Advection of North Atlantic Deep Water from the Labrador Sea to the southern hemisphere. Journal of Geophysical Research Oceans 120:2471–2487. http://dx.doi.org/10.1002/2014JC010605.
Richardson, M.J., 1987. Particle size, light scattering and composition of suspended particulate matter in the North Atlantic. Deep-Sea Res. 34, 1301–1329.
Richardson, M.J., Gardner, W.D., 1985. Analysis of suspended-particle-size distributions over the Nova Scotian continental rise. Mar. Geol. 66, 189–203.
Richardson, M.J., Wimbush, M., Mayer, L., 1981. Exceptionally strong near-bottom flows on the continental rise of Nova Scotia. Science 213, 887–888.
Richardson, M.J., Biscaye, P.E., Gardner, W.D., Hogg, N.G., 1987. Suspended particulate matter transport through the Vema channel. Mar. Geol. 77, 171–184.
Richardson, M.J., Weatherly, G.L., Gardner, W.D., 1993. Benthic storms in the Argentine Basin. Deep-Sea Res. 40, 975–987.
Sandwell, D.T., Zhang, B., 1989. Global mesoscale variability from Geosat Exact Repeat Mission: correlation with ocean depth. J. Geophys. Res. 94, 17971–17984.
Savidge, D.K., Bane, J.M., 1999. Cyclogenesis in the deep ocean beneath the Gulf Stream. J. Geophys. Res. 104, 18,111–18,126.
Schmitz, W.J., 1984. Abyssal kinetic energy in the North Atlantic. J. Mar. Res. 42, 509–536.
Shay, T.S., Bane, J.M., Watts, D.R., Tracey, K.L., 1995. Gulf Stream flow field and events near 68° W. J. Geophys. Res. 100, 22,565–22,589.
Smith, J.N., Smethie Jr., W.M., Yashayev, I., Curry, R., Azetsu-Scott, K., 2016. Time series measurements of transient tracers and tracer-derived transport in the Deep Western Boundary Current between the Labrador Sea and the subtropical Atlantic Ocean at Line W. Journal of Geophysical Research Oceans 121. http://dx.doi.org/10.1002/2016JC011759.
Sternberg, R.W., 1971. Measurements of incipient motion of sediment particles in the marine environment. Mar. Geol. 10, 113–119.
Thompson, R., 1971. Topographic Rossby waves at a site north of the Gulf Stream. Deep-Sea Res. 18, 1–19.
Thompson, R., 1977. Observations of Rossby waves near Site D. Prog. Oceanogr. 7, 135–162.
Thompson, R., Luyten, J., 1976. Evidence for bottom-trapped topographic Rossby waves from single moorings. Deep-Sea Res. 23, 629–635.
Thorndike, E.M., 1975. A deep-sea photographic nephelometer. Ocean Eng. 3, 1–15.
Tucholke, B.E., 1975. Sediment distribution and deposition by the western Boundary Undercurrent: the Greater Antilles Outer Ridge. J. Geol. 83, 177–207.
Tucholke, B.E., Eittreim, S., 1974. The western boundary undercurrent as a turbidity maximum over the Puerto Rico Trench. J. Geophys. Res. 79, 4115–4118.
Tucholke, B.E., Shirley, D.J., 1979. Comparison of laboratory and in situ compressional-wave velocity measurements on sediment cores from the western North Atlantic. J. Geophys. Res. 84, 687–695.
Tucholke, B.E., Wright, W.R., Hollister, C.D., 1973. Abyssal circulation over the Greater Antilles Outer Ridge. Deep-Sea Res. 20, 973–995.
Tucholke, B.E., Hollister, C.D., Biscaye, P.E., Gardner, W.D., 1985. Abyssal current character determined from sediment bedforms on the Nova Scotian continental rise. Mar. Geol. 66, 43–57.
Turnewitsch, R., Falahat, S., Nycander, J., Dale, A., Scott, R.B., Furnival, D., 2013. Deep-sea fluid and sediment dynamics—influence of hill- to seamount-scale seafloor topography. Earth Sci. Rev. 127, 203–241.
Watts, D.R., Tracey, K.L., Bane, J.M., Shay, T.J., 1995. Gulf Stream path and thermocline structure near 74°W and 68°W. Journal of Geophysical Research, Oceans 100, 18,291–18,312.
Watts, D.R., Qian, X., Tracey, K.L., 2001. Mapping abyssal current and pressure fields under the meandering Gulf Stream. J. Atmos. Ocean. Technol. 18, 1052–1067.
Weatherly, G.L., 1984. An estimate of bottom frictional dissipation by Gulf Stream fluctuations. J. Mar. Res. 42, 289–301.
Weatherly, G.L., Kelley, E.A., 1985. Two views of the cold filament. J. Phys. Oceanogr. 15, 68–81.
Welsh, E.B., Hogg, N.G., Hendry, R.M., 1991. The relationship of low-frequency deep variability near the HEBBLE site to Gulf Stream fluctuations. Mar. Geol. 99, 303–317.
Wishner, K.F., Gowing, M.M., 1992. The role of deep-sea zooplankton in carbon cycles. Deep-sea Food Chains and the Global Carbon CycleNATO ASI Series. Kluwer Academic Publishers, Netherlands, pp. 29–43.
Worthington, L.V., 1976. On the North Atlantic circulation. The Johns Hopkins Oceanographic Studies 6 (110 pp).
Wright, C.J., Scott, R.B., Furnival, D., Ailliot, P., Vermet, F., 2013. Global observations of ocean-bottom subinertial current dissipation. J. Phys. Oceanogr. 43:402–417. http://dx.doi.org/10.1175/JPO-D-12-082.1.
Wunsch, C., Grant, B., 1982. Towards the general circulation of the North Atlantic Ocean. Prog. Oceanogr. 11, 1–59.
Wyrtki, K., Magaard, L., Hager, J., 1976. Eddy energy in the oceans. J. Geophys. Res. 81, 2641–2646.